Volume 7 Number 4 Oct - Dec 2018

STUDENT JOURNAL OF PHYSICS

INTERNATIONAL JOURNAL

INDIAN ASSOCIATION OF PHYSICS TEACHERS

ISSN – 2319-3166

STUDENT JOURNAL OF PHYSICS

This is a quarterly journal published by Indian Association Of Physics Teachers. It publishes research articles contributed by Under Graduate and Post Graduate students of colleges, universities and similar teaching institutions, as principal authors.

Registered Office

Editor-in-Chief, SJP, Institute of Physics, Sainik School, Bhubaneswar, Odisha, India – 751005
(www.iopb.res.in/~sjp/)

STUDENT JOURNAL OF PHYSICS

Scope of the Journal

The journal is devoted to research carried out by students at undergraduate level. It provides a platform for the young students to explore their creativity, originality, and independence in terms of research articles which may be written in collaboration with senior scientist(s), but with a very significant contribution from the student. The articles will be judged for suitability of publication in the following two broad categories:

1. **Project based articles**
   These articles are based on research projects assigned and guided by senior scientist(s) and carried out predominantly or entirely by the student.
2. **Articles based on original ideas of student**
   These articles are originated by the student and developed by him/ her with possible help from senior advisor. Very often an undergraduate student producing original idea is unable to find a venue for its expression where it can get due attention. SJP, with its primary goal of encouraging original research at the undergraduate level provides a platform for bringing out such research works.
   It is an online journal with no cost to the author.

Since SJP is concerned with undergraduate physics education, it will occasionally also publish articles on science education written by senior physicists.

Information for Authors

- Check the accuracy of your references.
- Include the complete source information for any references cited in the abstract. (Do not cite reference numbers in the abstract.)
- Number references in text consecutively, starting with [1].

- Language: Papers should have a clear presentation written in good English. Use a spell checker.

Submission

1. Use the link "Submit" of Website to submit all files (manuscript and figures) together in the submission (either as a single .tar file or as multiple files)
2. Choose one of the Editors in the link "Submit" of Website as communicating editor while submitting your manuscript.

Preparation for Submission

Use the template available at "Submit" section of Website for preparation of the manuscript.

Re-Submission

- For re-submission, please respond to the major points of the criticism raised by the referees.
- If your paper is accepted, please check the proofs carefully.

Scope

- SJP covers all areas of applied, fundamental, and interdisciplinary physics research.

A device for generating collimated polychromatic light and for concentrating scattered light from a fluid

Dhiman Biswas[1]
[1]B.Sc Physics, Ramakrishna Mission Residential College (Narendrapur)

Abstract. Here we have designed a device that can collect most of the light emitted by a long cylindrical source of polychromatic light and collimate it in a intense narrow beam of light. Different possible aberration are taken care of and losses are considered. We discuss an important application of this design concentrating scattered light coming from a fluid, for example in the case of Raman scattering.
Keywords. Intense collimated polychromatic beam, scattered light from a fluid, Huygens principle in cylindrical symmetry.

1. INTRODUCTION

Light and its strange behaviors have astonished physicists for centuries. From the very early days of Newton, optical experiments have become an essential part of physics. One equipment that is essential for most of the optical experiments is a white light source. And most often it also needs to be a source of parallel beams.

To get a light source like this, is not so easy. There are some conventional methods with a pin hole and collimators but they are not that efficient. One actually eliminates about 95% of the light that is emitted by the main source like a filament bulb or a gas tube, so the 95% of the electrical energy that we put in is also wasted. Importantly, the resulting source is of very low intensity, because of which the observations become very difficult and inefficient.

Here I have designed an equipment that can give us highly intense white light source utilizing most of the energy radiated from the main source as light. We will discuss that this devices light gathering ability can be very useful for certain cases like Raman's scattering experiment where we have to do spectral analysis of light scattered from a liquid. As the scattered intensity varies as $\frac{1}{\lambda^4}$ it becomes very difficult to do the measurements in high wavelength range. Here using this device we can have the maximum intensity possible.

2. WAVEFRONTS DUE TO AN INFINITELY LONG PERFECTLY CYLINDRICAL LIGHT SOURCE

If we consider an infinitely long cylindrical light source of coherent light then, according to Huygen's principle [1], each point on its surface would act as a secondary source. The secondary wavelets generated from those points would eventually superpose and create another wave front of

same phase at λ distance apart. Now as shown in Fig.1 all the wavefronts will be coaxial cylinders and the rays will be perpendicular to the wavefronts hence with the axis. This is kind of obvious because as there is cylindrical symmetry the rays will not know any other direction except radial direction. First we will discuss this situation and discuss creation of collimated light from such a source. This situation will be useful for concentrating light scattered from fluids using a laser light source (as for Raman scattering experiments) as we will discuss in section 4. Later we will discuss that even for incoherent light, the geometry of the set up should lead to significantly intense collimated light beams.

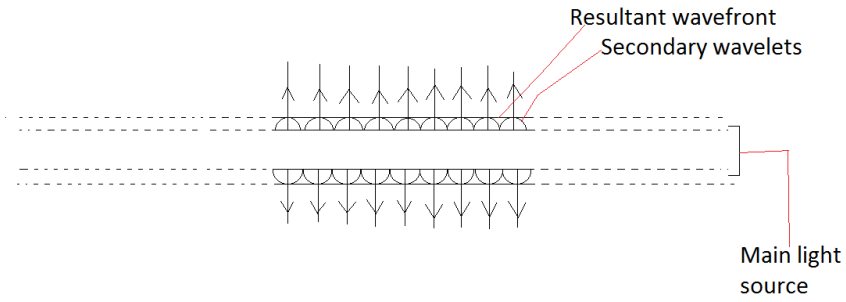

Figure 1. Wavelets and wave fronts for a cylindrical source of coherent light

3. DESIGN FOR COLLIMATED LIGHT SOURCE

The design for collimated intense light source has two parts i) Concentration of incoming parallel beams as efficiently as possible. ii) Production of parallel beams from a perfectly cylindrical gas tube. We will discuss each of them in details below.

For efficient concentration of incoming parallel beams, the usual method of doing this uses two lenses of different focal lengths. One lens has be of larger aperture than other. They must be aligned in such a way that the rays get focused in the focus point of smaller lens by the larger lens. This setup suffers from chromatic aberration as the focal length for different colors would be different (unless one is using achromatic lens combinations). Though for usual laboratory experiments the aberration can be neglected but it is better to use parabolic mirrors. In our setup we will use the parabolic mirror so the issue of spherical aberration is also eliminated [2]. The arrangement of mirrors is shown in the Fig.2. The calculation for output intensity with respect to the intensity of incident ray is shown below.

According to the polar equation of parabola

$$r = \frac{2f}{1 - cos\phi} \tag{1}$$

Now here $OA = r_2$ and $OB = r_1$ as shown in Fig.2 (taking the focus of each parabola to be the same point.)

$$Now \;\; r_2 = \frac{2f_2}{1 - cos(\phi)} \;\; for \;\; secondary \;\; mirror$$

$$r_1 = \frac{2f_1}{1 - cos(\phi)} \;\; for \;\; primary \;\; mirror$$

Now clearly

$$\frac{r_2}{r_1} = \frac{f_2}{f_1} \tag{2}$$

And also

$$\frac{r_2}{r_1} \simeq \frac{a_2}{a_1} \tag{3}$$

Now from equation(2) and equation(3)

$$\frac{f_2}{f_1} = \frac{a_2}{a_1}$$

And we also know that $I \propto \frac{1}{a^2}$, so we can write:-

$$I_2 = I_1(\frac{f_1}{f_2})^2$$

Here:- f_i= focal length of ith mirror
And a_i= aperture of ith mirror
I_1= intensity of incoming beam
I_2=intensity of outgoing beam

Now we will discuss how to produce parallel beams from a long cylindrical light source.

Main part of the device is conical mirror of angle 45° and a long cylindrical light source. The arrangement is shown in the Fig.3. Here we have to keep one thing in mind that the diameter of the cylindrical gas tube should small compared to its length (say, less than 5% of its length). This has to be done because the cylindrical source is of finite length and to minimize its edge effect this source have to be very thin compared to its length. The full setup has three parts as shown in Fig.3, the parallel beam emitter, absorber of imperfections and concentrator. As we discussed earlier, cylindrical source will lead to emission of rays which are normal to the cylindrical axis (for coherent light source). 45° angle conical mirror will convert these rays into parallel light beam. The absorber of imperfections part is actually a cylindrical channel between other two remaining

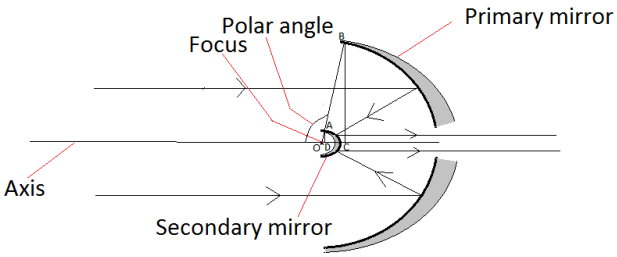

Figure 2. Arrangement of the mirrors for the concentrator

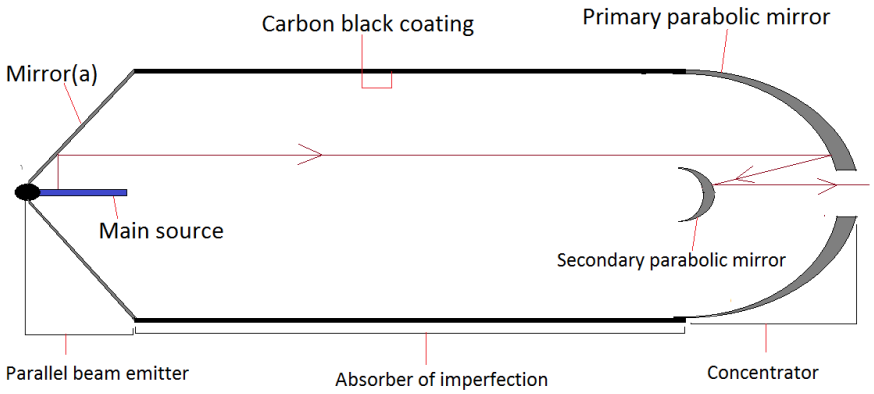

Figure 3. The device

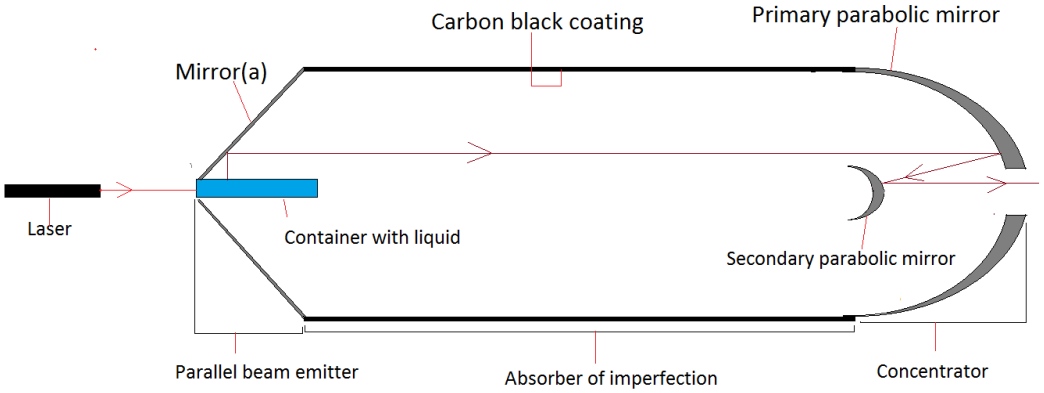

Figure 4. Modified setup for concentrating scattered light from a fluid, e.f. for Raman scattering

parts with carbon black coating on the wall. The middle part is there to absorb all the rays that are not parallel to the axis of the whole device thus eliminating the imperfections. This will take care of the edge effects when the cylindrical light source is coherent. For incoherent cylindrical light source there will be a good fraction of light even from the cylindrical part which will not form parallel beam and this middle portion will absorb all that. Basically, for incoherent light source, the use of cylindrical geometry of light source will help in getting strong intensity for parallel beam. This parallel beam will then be focused by the third part which is the parabolic concentrator finally leading to intense thin collimated light source. As we mentioned, use of parabolic mirrors eliminates chromatic aberration hence white light source (as from a tubelight) can also be used to get collimated white light beam.

4. MODIFIED VERSION OF THE DEVICE FOR CONCENTRATING SCATTERED LIGHT FROM A FLUID

We now discuss an important application of this device for experiments where one has to study the spectrum of scattered light from a fluid, like the experiment of Raman Effect. For this purpose, we replace the main cylindrical light source of Fig.3 (e.g. gas tube) with a cylindrical cylindrical container with the sample fluid. (The setup will work for the liquid sample as well as gas sample.) One plane of the container will be transparent and the liquid will be illuminated by a high intensity laser beam through that side. Now the liquid will act as a new cylindrical source, with the scattered light emanating from the tube propagating in the perpendicular direction to the cylindrical axis (as discussed in Sec.1). Rest of the mechanism is same as in Fig.2. Here all the scattered light will be gathered and concentrated to a thin intense beam. The original laser light propagating along the cylindrical axis should be absorbed either at the end of the tube containing the fluid, or at the

back of the parabolic mirrors (with appropriate black coatings). The final collimated beam emerging from the parabolic concentrators will almost entirely consist of the light scattered from the liquid, significantly increasing the intensity of the scattered light for experimental analysis. The schematic diagram of the arrangement is shown in Fig.4.

One experiment that can get benefited from this device is the Raman's scattering experiment. We know that the intensity of Raman lines is very low especially the anti stokes line as the probability of anti Stoke transition is very low [2]. So if we use this device we can measure the wavelength of those lines more efficiently. Many other UV and NIR based spectroscopies can also get benefited from this device as they also face similar kind of problems due to low transition probability of certain lines.

5. DISCUSSION AND CONCLUSIONS

There are several points one needs to be careful about for efficient functioning of this device. The main light source has to be perfectly cylindrical for the main argument of Sec.1 to hold. Also, the diameter of the circular cross-section of the cylindrical light source must be small compared to the length of the cylinder. This is because the wave front emitting from the gas tube is assumed to be perfectly cylindrical but in reality there will be slight curvature at the edges of the cylindrical wave front. To minimize this, the gas tube has to be made longer in compare to its diameter. Again, we emphasize that the argument of Sec.1 holds for coherent light source. For Raman scattering experiment (as discussed for the modified device in Sec.3) where original source is a laser, the scattered light will have strong coherent component, hence the device should work efficiently for that. Even for incoherent light source (such as ordinary tubelight for white light source), the geometry of the device (with long cylindrical source and 45° conical mirror) one should expect production of intense collimated beam. One important part of the device is the mid section which has to be coated black to absorb all the imperfect rays. So the mid section of the device has to be sufficiently long enough to make sure that the rays that are reaching the concentrator are almost parallel to the axis of the device. It should be clear that this design will work perfectly for sound waves as well. For reasonable size of the device, one can have cylindrical source of ultrasonic waves (having coherent source will be easy for sound waves). Then, with all the reflectors designed for sound waves, the device should be able to produce thin collimated beam of ultrasonic waves which can have many applications.

6. ACKNOWLEDGMENT

I gratefully acknowledge the help of Dr Sourav Chattopadhay, professor of Ramakrishna Mission Residential College(Narendrapur) and I would also like to show gratitude to Dr. Ajit Srivastava, my mentor of NIUS project for encouraging me in this path of innovation and exploration and helping me in writing this report.

References

[1] Ajoy Ghatak, ”Optics”, 6th edition, McGraw Hill Education India Private Limited

[2] Wikipedia, https://www.wikipedia.org

STUDENT JOURNAL OF PHYSICS

The effect of right-handed currents and dark side of the solar neutrino parameter space to Neutrinoless Double Beta Decay

Pritam Kumar Bishee[1] *, **Purushottam Sahu**[2] †, **Sudhanwa Patra**[2] ‡
1. Integrated M.Sc. 3^{rd} Year, National Institute of Technology, Rourkela, Odisha, India
2. Indian Institute of Technology Bhilai, Raipur 492015, Chhattisgarh, India

Abstract. We discuss how dark side of the solar neutrino parameter space and effect of new physics contributions from right-handed currents can reveal the Majorana nature of neutrinos by the observation of the rare process called neutrinoless double beta decay, i.e. the simultaneous decay of two neutrons in the nucleus of an isotope (A, Z) into two protons and two electrons without the emission of any neutrinos i.e.$(A, Z) \rightarrow (A, Z + 2) + 2e^{-}$. While the standard mechanism of neutrinoless double beta decay with exchange of light Majorana neutrinos, normal ordering and inverted ordering can not saturate the present experimental limit, and quasi-degenerate light neutrinos are strongly disfavored by cosmology, we consider new physics contributions due to right-handed charged current effects arising in TeV scale left-right symmetric model which can satuare the experimental bound provided by KamLAND-Zen and GERDA.

Keywords: Solar Neutrino, Neutrinoless double beta decay, Majorana neutrinos.

1. INTRODUCTION

The recent neutrino oscillation experiments revealed that neutrinos have non-zero masses and mixing, which calls for new physics beyond the standard model as the standard model of particle physics predicts massless neutrinos. On the other hand, neutrinoless double beta decay($0\nu\beta\beta$) is a unique phenomenon whose experimental observation would reveal whether neutrinos are Majorana particles [1] which violates Lepton Number. Majorana particles are their own antiparticles. All the fermions present in the standard model are of Dirac type and only the neutrino, being neutral, can become the Majorana particle. The main parameter of $0\nu\beta\beta$ is effective Majorana mass(m_{ee}) that depends upon the absolute mass and mass ordering of the neutrino i.e. whether the neutrino mass follows normal ordering (NO) in which third mass eigenstate is the heaviest or inverted ordering (IO) in which the third mass eigenstate is lightest. This process also has the potential to tell us about the absolute mass scale and mass ordering of neutrino. So Scientists around the world are putting in enormous effort, and different experiments are going on to tell us about $0\nu\beta\beta$ process. No positive signal has been observed yet in any of the experiment. But lower limit on the half-life

*e-mail:pritamkumarbishee@gmail.com
†purushottams@iitbhilai.ac.in
‡sudhanwa@iitbhilai.ac.in

($T_{1/2}$) on neutrinoless double beta decay of different isotope i.e. $T_{1/2}(Xe^{156}) > 1.5 \times 10^{25}$yrs from KAMLAND-Zen[39], $T_{1/2}(Ge^{76}) > 8 \times 10^{25}$yrs from GERDA[46] and $T_{1/2}(Te^{130}) > 1.5 \times 10^{25}$ yrs from the combined result of CURCINO & CUORE[41] has been found with 90% C.L .

The discovery of neutrino oscillation, which gives the evidence of neutrino masses and mixing, has an enormous impact on our perception about the understanding of the universe. In the study of particle physics, the most successful and well-accepted theory is the standard model (SM) of the particle physics that has been found to agree with almost all experimental data up to current accelerator energy. All of the particles present in the SM have been experimentally observed. Despite the immense success of the SM, it fails to explain some of the fundamental questions like non zero neutrino mass, the mystery of dark matter and matter-antimatter asymmetry of the universe. So we have to think beyond the standard model (BSM) of particle physics to explain all the shortcoming of SM.
A well-motivated candidates of physics beyond the standard model is Left-Right Symmetric Model (LRSM)[33–36]. It contains additional right-handed current compare to the SM. It explains light neutrino mass via seesaw mechanism by normally adding right-handed neutrino to the model which are absent in the SM of particle physics. It also provides the theoretical origin of maximal parity violation which is observed in weak interactions while remaining conserved in strong and electromagnetic interactions. It is based on the gauge group $SU(3)_C \times SU(2)_L \times SU(2)_R \times U(1)_{B-L}$. Here the right-handed neutrino is the necessary part of the model. Neutrinos acquire their mass from both Type-I and Type-II seesaw mechanism that arises naturally in the LRSM.

Neutrino oscillation experiments provide information about mass squared differences and mixing angles i.e. ($\Delta m^2, sin^2 2\theta$). Here we always use ($0 \leq \theta \leq \pi/4$), which is called the "light side" of the parameter space. However, it misses the other half of the parameter space ($\pi/4 < \theta \leq \pi/2$), which is called the "dark side"[44]. Neutrino oscillation in vacuum depends on $sin^2 2\theta$, which is equivalent for both light and dark sides of the parameter space. That's why we only use the light side of the parameter space. But in the case of matter effect i.e. non-standard neutrino interactions (NSI)[42, 43], the dark side and the light side are physically inequivalent. The light side solution to the solar neutrino problem is generally called standard large mixing angle i.e LMA solution, whereas the dark side solution to the solar neutrino problem is called as Dark-LMA i.e DLMA solution.

In this paper, we study the effect of DLMA solution to the solar neutrino problem on neutrinoless double beta ($0\nu\beta\beta$) decay for both of these standard and right-handed current mechanisms and compare them with the standard LMA solution to the solar neutrino problem on $0\nu\beta\beta$ for both mechanisms. This knowledge will help the future experiments to probe different energy range of effective mass and find out the sensitivity on $0\nu\beta\beta$.

2. STANDARD MECHANISM OF NEUTRINOLESS DOUBLE BETA DECAY

Standard model of particle physics is based on the gauge group $SU(3)_C \times SU(2)_L \times U(1)_Y$. It contains only left-handed neutrino. Right-handed neutrino is absent in the standard model of particle physics. Different experiments have found the half-life of different isotopes for $0\nu\beta\beta$. So for standard mechanism, the inverse half-life ($T_{1/2}$) for $0\nu\beta\beta$ is given as

$$[T_{1/2}]^{-1} = G \left| \frac{M_\nu}{m_e} \right|^2 |m_{ee}^\nu|^2 \tag{1}$$

where G is the phase factor, M_ν is the nuclear matrix element, m_e is the mass of electron and m_{ee}^ν is the effective majorana mass. We know the value of G and M_ν of different isotopes. So the main parameter of interest in $0\nu\beta\beta$ is the effective majorana mass(m_{ee}^ν) which is the combination of neutrino mass eigenvalues and neutrino mixing matrix element. The effective majorana mass is given by

$$m_{ee}^\nu = \left| \sum_{i=1}^{3} U_{ei}^2 m_i \right| \tag{2}$$

where U is the unitary PMNS mixing matrix and m_i is the mass eigenvalues.
PMNS mixing matrix U is given by

$$U = \begin{pmatrix} 1 & 0 & 0 \\ 0 & c_{23} & s_{23} \\ 0 & -s_{23} & c_{23} \end{pmatrix} \begin{pmatrix} c_{13} & 0 & s_{13}e^{-i\delta} \\ 0 & 1 & 0 \\ -s_{13}e^{i\delta} & 0 & c_{13} \end{pmatrix} \begin{pmatrix} c_{12} & s_{12} & 0 \\ -s_{12} & c_{12} & 0 \\ 0 & 0 & 1 \end{pmatrix} \begin{pmatrix} 1 & 0 & 0 \\ 0 & e^{\frac{i\alpha}{2}} & 0 \\ 0 & 0 & e^{\frac{i\beta}{2}} \end{pmatrix} \tag{3}$$

where $c_{ij} = \cos\theta_{ij}, s_{ij} = \sin\theta_{ij}$,$\delta$ is the CP violation phases and α, β are majorana phases.
if we put the value of mixing matrix U in eq.2 , then effective mass is

$$m_{ee}^\nu = \left| m_1 c_{12}^2 c_{13}^2 + m_2 s_{12}^2 c_{13}^2 e^{i\alpha} + m_3 s_{13}^2 e^{i\beta} \right| \tag{4}$$

Here, the effective mass depends upon the neutrino oscillation parameter θ_{12},θ_{13} and the neutrino mass eigenvalues m_1, m_2 and m_3 for which we don't know the absolute value but we know the mass squared differences between them. and we don't know anything about the majorana phases.
we know the value of Δm_{sol}^2, which is $\Delta m_{sol}^2(\Delta m_{21}^2) = m_2^2 - m_1^2$, it has a positive sign so always $m_2 > m_1$. and we don't know the sign of $m_{atm}^2(\Delta m_{31}^2)$, which allows for two possible ordering of neutrino mass i.e.

$$\begin{aligned} \Delta m_{atm}^2(\Delta m_{31}^2) &= m_3^2 - m_1^2, \text{for Normal Ordering(NO)} \\ &= m_1^2 - m_3^2, \text{for Inverted Ordering(IO)} \end{aligned}$$

Normal Ordering (NO) : $m_1 < m_2 << m_3$

$$\text{Here, } m_1 = m_{\text{lightest}} \text{ ; } m_2 = \sqrt{m_1^2 + \Delta m_{sol}^2} \text{ ;}$$
$$m_3 = \sqrt{m_1^2 + \Delta m_{sol}^2 + \Delta m_{atm}^2} \tag{5}$$

Inverted Ordering (IO) : $m_3 << m_1 < m_2$

$$\text{Here, } m_3 = m_{\text{lightest}} \text{ ; } m_1 = \sqrt{m_3^2 + \Delta m_{atm}^2} \text{ ;}$$
$$m_2 = \sqrt{m_3^2 + \Delta m_{atm}^2 + \Delta m_{sol}^2} \tag{6}$$

Oscillation Parameters	within 3σ range ([29])
$\Delta m_{21}^2[10^{-5}\text{eV}^2]$	7.05-8.14
$\lvert\Delta m_{31}^2(\text{NO})\rvert[10^{-3}\text{eV}^2]$	2.41-2.60
$\lvert\Delta m_{31}^2(\text{IO})\rvert[10^{-3}\text{eV}^2]$	2.31-2.51
$\sin^2\theta_{12}$	0.273-0.379
$\sin^2\theta_{13}(\text{NO})$	0.0196-0.0241
$\sin^2\theta_{13}(\text{IO})$	0.0199-0.0244

Table 1. The oscillation parameters like mass squared differences and mixing angles within 3σ range.[29]

In this paper, we symbolize θ_{D12} for the DLMA solution in presence of NSI and θ_{12} as the standard LMA solution. The 3σ range of both θ_{12} and θ_{D12} are given in Table.2 [29, 30]. By varying all the neutrino oscillation parameters in their 3σ ranges and varying the Majorana phases α and β from 0 to 2π range, we obtained the plot of effective mass as a function of lightest neutrino mass i.e. m_1,m_3 for NO and IO respectively in Fig.1 .

We plot the effective mass by putting LMA and DLMA solution for both NO and IO in Fig.1. Here, the gray band($0.07 - 0.16$ eV) refers to the current upper limit obtained from the combined result of KamLAND-Zen and GERDA[46]. The region above this is disallowed. and the yellow region is disallowed by the cosmological constraints on the sum of light neutrino masses[31] .

From the Fig.1, For NO, we found out that m_{ee}^{ν} for the DLMA solution is shifting into the region between the NO and IO of LMA solution which is called as the desert region and m_{ee}^{ν} for

	$sin^2\theta_{12}$	$sin^2\theta_{D12}$
min	0.273	0.650
max	0.379	0.725

Table 2. LMA and DLMA solution for θ_{12} to the solar neutrino problem.

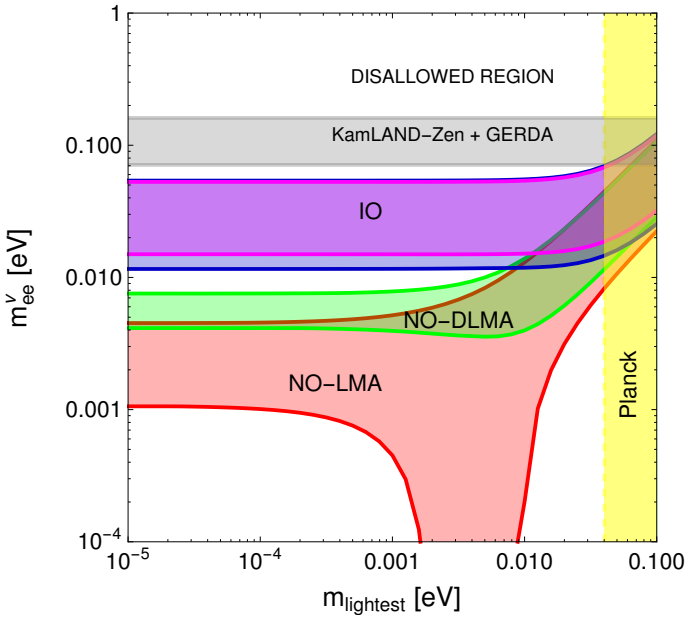

Figure 1. Effective majorana mass m^{ν}_{ee} for neutrinoless double beta decay as a function of lightest neutrino mass for standard mechanism. Here the red and green band correspond to the solution of θ_{12} and θ_{D12} for NO , blue and magenta band correspond to the solution of θ_{12} and θ_{D12} for IO.

the DLMA solution is found out to be higher than that of LMA solution. and when the $m_{\rm lightest}$ increases, the overlap region between the LMA and DLMA solution also increases. For $m_{\rm lightest} \in [10^{-3}, 10^{-2}]$eV, we found that the minimum value of m^{ν}_{ee} for LMA solution is very small i.e. it nearly vanishes. But for DLMA solution, in that region the minimum value of m^{ν}_{ee} remains the same as the value when $m_{\rm lightest} < 10^{-3}$eV for NO.

But in case of IO, the maximum value of m^{ν}_{ee} for both LMA and DLMA solution remain same. whereas the minimum value of m^{ν}_{ee} for DLMA solution is slightly higher than the LMA solution which is nearly same. The overlap region between LMA and DLMA solution remains the same throughout the value of $m_{\rm lightest}$. Here The DLMA solution fully overlaps with the LMA solution. No considerable change is found between both of these solutions for IO. So m^{ν}_{ee} remains the same for both LMA and DLMA solution in IO.

3. RIGHT-HANDED CURRENT EFFECTS TO NEUTRINOLESS DOUBLE BETA DECAY

We believe that lepton number violating $0\nu\beta\beta$ transitions could be induced either by standard mechanism due to the exchange of light Majorana neutrinos discussed in previous section or by corresponding new interactions. Since we have already found that standard mechanism can not saturate the present experimental bound one has to go beyond SM framework and there exist many models contributing to neutrinoless double beta decay [2–5, 11, 15, 17, 18, 20, 22, 23, 26]. In the present work, we have considered new interactions arising from purely right-handed currents within left-right symmetric models – parametrized in terms of the effective mass parameter or the half-life of the nucleus – which can saturate the current experimental bounds and one can derive limits for light Majorana neutrino masses, right-handed Majorana neutrinos, right-handed charged gauged boson mass M_{W_R} and its mixing with the left-handed counterpart gauge boson and the corresponding gauge coupling g_R.

We consider a left-right symmetric model with Type-II seesaw dominance[32, 37, 38] where symmetry breaking occurred at TeV scale leading to right-handed charged gauge boson W_R and right-handed neutrino N_R mass in the order of TeV scale. This leads to new physics contribution to $0\nu\beta\beta$ due to right-handed current via $W_R - W_R$ mediation and heavy neutrino exchange.

When we considered LRSM with Type-II seesaw dominance, the mass eigenvalues of the left and right handed neutrinos are proportional to each other,

$$m_L \propto M_R \tag{7}$$

As a result of this, the left and right handed neutrinos have the same PMNS mixing matrix.

$$U_L^{PMNS} = V_R^{PMNS} \tag{8}$$

and the mass eigenvalues are related as follows: **Normal Ordering (NO)**($m_1 = m_{\rm lightest}$)

$$m_2 = \sqrt{m_1^2 + \Delta m^2_{sol}}\,;\; m_3 = \sqrt{m_1^2 + \Delta m^2_{sol} + \Delta m^2_{atm}}\,,$$

$$M_1 = \frac{m_1}{m_3} M_3 \; ; \; M_2 = \frac{m_2}{m_3} M_3 \tag{9}$$

Here we fixed the heaviest right-handed neutrino mass M_3 for NO.

Inverted Ordering (IO)($m_3 = m_{\rm lightest}$)

$$m_1 = \sqrt{m_3^2 + \Delta m_{atm}^2} \; ; \; m_2 = \sqrt{m_3^2 + \Delta m_{atm}^2 + \Delta m_{sol}^2} \, ,$$

$$M_1 = \frac{m_1}{m_2} M_2 \; ; \; M_3 = \frac{m_3}{m_2} M_2 \tag{10}$$

Here we fixed the heaviest right-handed neutrino mass M_2 for IO.

When we considered the LRSM with Type-II see saw dominance where the effect of purely right handed current along with standard mechanism is taken into consideration, the inverse half-life of a given isotope for $0\nu\beta\beta$ is given by

$$\begin{aligned} [T_{1/2}]^{-1}_{LR} &= G \left| \frac{M_\nu}{m_e} \right|^2 (|m^\nu_{ee}|^2 + |m^N_{ee}|^2) \\ &= G \left| \frac{M_\nu}{m_e} \right|^2 |m^{\nu+N}_{ee}|^2 \end{aligned} \tag{11}$$

where m^ν_{ee} is the effective mass arising due to left-handed neutrino in standard mechanism and m^N_{ee} is the effective mass arising due to purely right handed current. Also, here $|m^{\nu+N}_{ee}|^2 = |m^{LR}_{ee}|^2 = |m^\nu_{ee}|^2 + |m^N_{ee}|^2$,where m^{LR}_{ee} is the total effective mass arising due to right-handed current in LRSM. We know the expression for m^ν_{ee} that is given in eq.4 and the expressions for m^N_{ee} is given by

$$\begin{aligned} m^N_{ee} &= \frac{C_N}{M_3} \left| c^2_{12} c^2_{13} \frac{m_3}{m_1} + s^2_{12} c^2_{13} \frac{m_3}{m_2} e^{i\alpha} + s^2_{13} e^{i\beta} \right| \text{ (NO)} \\ &= \frac{C_N}{M_2} \left| c^2_{12} c^2_{13} \frac{m_2}{m_1} + s^2_{12} c^2_{13} e^{i\alpha} + s^2_{13} \frac{m_2}{m_3} e^{i\beta} \right| \text{ (IO)} \end{aligned}$$

where $C_N = \langle p^2 \rangle \left(\frac{g_R}{g_L}\right)^4 \left(\frac{M_{W_L}}{M_{W_R}}\right)^4$. Here typical momentum transfer $\langle p \rangle \approx 100$ MeV , g_R & g_L are the coupling constants of $SU(2)_L$ & $SU(2)_R$ respectively and M_{W_L} & M_{W_R} are the masses of the left and right-handed gauge bosons i.e W_L and W_R respectively that mediate the process. In this paper, we denote M_N as the heaviest right-handed neutrino mass eigenvalue i.e. M_3 for NO and M_2 for IO.

In the present work, we have considered $g_R \approx g_L$,$M_N = 1$ TeV,$M_{W_L} = 80.379$ GeV and $M_{W_R} \approx 3.5$ TeV [45]. By varying all the oscillation parameters in their 3σ range[29] and Majorana phases from 0 to 2π, we obtained the plot of effective mass (m^{LR}_{ee}) as a function of lightest neutrino mass for NO and IO by using both LMA and DLMA solution in Fig.2 .

From the Fig.2, For NO, we found that the effective mass(m^{LR}_{ee}) remains nearly the same for the higher value of absolute mass i.e. $m_{\rm lightest} > 0.03$ eV, but that region is disfavoured by the cosmological constraint. We observed that both the LMA and DLMA solutions for NO saturate the higher value of effective mass limit provided by KamLAND-Zen and GERDA so that we can

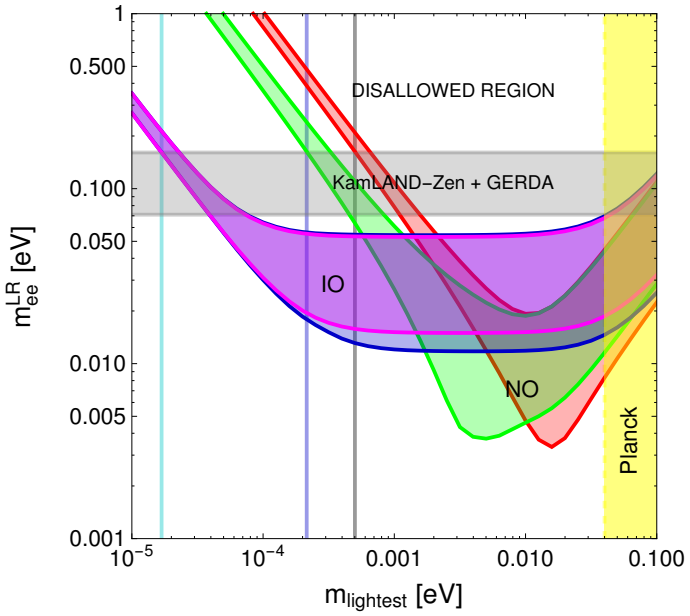

Figure 2. effective majorana mass m_{ee}^{LR} for neutrinoless double beta decay as a function of lightest neutrino mass from the contribution of right handed current.Here the red and green band correspond to the solution of θ_{12} and θ_{D12} for NO, blue and magenta band correspond to the solution of θ_{12} and θ_{D12} for IO.

find the lower limit of absolute mass of the lightest neutrino. Here DLMA solution (Green band) is shifted towards the left as compared to the LMA solution (Red band) implying that the lower limit of absolute mass for DLMA solution is comparatively smaller than the lower limit of absolute mass for LMA solution. But the m_{ee}^{LR} range is the same for both of these solutions for NO. So the lower limit of absolute mass of the lightest neutrino for NO is found out to be

$$m_{\text{lightest}} > 5.01 \times 10^{-4} \text{ (for LMA solution)}$$

$$m_{\text{lightest}} > 2.15 \times 10^{-4} \text{ (for DLMA solution)}$$

In case of IO, m_{ee}^{LR} remains the same for both LMA and DLMA solutions. So both of these solutions are equal for IO. Here also both of these solutions saturate the higher value of m_{ee}^{LR}. As both LMA and DLMA solutions are equal for IO, we found the same lower limit of m_{lightest} for both of these solutions. The lower limit of absolute mass of the lightest neutrino for IO is found to be

$$m_{\text{lightest}} > 1.685 \times 10^{-5} \text{ (IO)}$$

which is very small as compared to the lower limit of absolute mass of lightest neutrino for both LMA and DLMA solutions for NO.

4. CONCLUSION

If the $0\nu\beta\beta$ process happens, it will address many unsolved fundamental questions of physics like Majorana nature of the neutrino, matter-antimatter asymmetry, absolute mass scale and mass ordering of neutrino which will help us for the better understanding of the universe. So searching for this rare process is of paramount importance. From the standard mechanism, we found out that the DLMA solution for NO is shifting into the desert region ($0.004 - 0.0075$ eV) which provides a new sensitivity goal for the future experiments. If we find any positive signal for $0\nu\beta\beta$ in that desert region, this will confirm the DLMA solution to the solar neutrino problem as well. From the right-handed current mechanism, we found that both LMA and DLMA solutions to the solar neutrino problem for both NO and IO saturate the experimental limit provided by KamLAND-Zen and GERDA, which also provide the lower limit of absolute mass of lightest neutrino that is not provided by the standard mechanism. So if we find any positive signal for $0\nu\beta\beta$ above the region of IO in the standard mechanism, we have to consider the contribution from the right-handed current as well.

References

[1] Majorana, Ettore, Theory of the Symmetry of Electrons and Positrons, Nuovo Cim., 14, 1937, 171-184, 10.1007/BF02961314, RX-888

[2] Babu, K. S. and Mohapatra, R. N., New vector - scalar contributions to neutrinoless double beta decay and constraints on R-parity violation, Phys. Rev. Lett., 75, 1995, 2276-2279, 10.1103/PhysRevLett.75.2276, hep-ph/9506354, BA-95-15, UMD-PP-95-117

[3] Hirsch, M. and Klapdor-Kleingrothaus, H. V. and Kovalenko, S. G., New supersymmetric contributions to neutrinoless double beta decay, Phys. Lett., B352, 1995, 1-7, 10.1016/0370-2693(95)00460-3, hep-ph/9502315

[4] Hirsch, M. and Klapdor-Kleingrothaus, H. V. and Kovalenko, S. G., Supersymmetry and neutrinoless double beta decay, Phys. Rev., D53, 1996, 1329-1348, 10.1103/PhysRevD.53.1329, hep-ph/9502385

[5] Hirsch, M. and Klapdor-Kleingrothaus, H. V. and Kovalenko, S. G., New leptoquark mechanism of neutrinoless double beta decay, Phys. Rev., D54, 1996, 4207-4210, 10.1103/PhysRevD.54.R4207, hep-ph/9603213

[6] Ge, Shao-Feng and Rodejohann, Werner, JUNO and Neutrinoless Double Beta Decay, 2015, 1507.05514

[7] Mohapatra, Rabindra N. and Senjanović, Goran, Neutrino Mass and Spontaneous Parity Violation, Phys.Rev.Lett., 44, 912, 10.1103/PhysRevLett.44.912, 1980

[8] Senjanović, Goran, Spontaneous Breakdown of Parity in a Class of Gauge Theories, Nucl.Phys., B153, 334-364, 10.1016/0550-3213(79)90604-7, 1979

[9] Heeck, Julian and Patra, Sudhanwa, Minimal Left-Right Dark Matter, 2015, 1507.01584

[10] Patra, Sudhanwa and Queiroz, Farinaldo S. and Rodejohann, Werner, Stringent Dilepton Bounds on Left-Right Models using LHC data, 2015, 1506.03456

[11] Deppisch, Frank F. and Gonzalo, Tomas E. and Patra, Sudhanwa and Sahu, Narendra and Sarkar, Utpal, Double beta decay, lepton flavor violation, and collider signatures of left-right symmetric models with spontaneous D-parity breaking, Phys. Rev., D91, 2015, 1, 015018, 10.1103/PhysRevD.91.015018, 1410.6427

[12] Deppisch, Frank F. and Gonzalo, Tomas E. and Patra, Sudhanwa and Sahu, Narendra and Sarkar, Utpal, Signal of Right-Handed Charged Gauge Bosons at the LHC?, Phys. Rev., D90, 2014, 5, 053014, 10.1103/PhysRevD.90.053014, 1407.5384

[13] Patra, Sudhanwa and Pritimita, Prativa, Post-sphaleron baryogenesis and n - $\overline{n}$ oscillation in non-SUSY SO(10) GUT with gauge coupling unification and proton decay, Eur. Phys. J., C74, 2014, 10, 3078, 10.1140/epjc/s10052-014-3078-x, 1405.6836

[14] Borah, Debasish and Patra, Sudhanwa and Pritimita, Prativa, Sub-dominant type-II seesaw as an origin of non-zero θ_13 in SO(10) model with TeV scale Z' gauge boson, Nucl. Phys., B881, 2014, 444-466, 10.1016/j.nuclphysb.2014.02.017, 1312.5885

[15] Awasthi, Ram Lal and Parida, M.K. and Patra, Sudhanwa, Neutrino masses, dominant neutrinoless double beta decay, and observable lepton flavor violation in left-right models and SO(10) grand unification with low mass W_R, Z_R bosons, JHEP, 1308, 122, 10.1007/JHEP08(2013)122, 2013, 1302.0672

[16] Patra, Sudhanwa, Neutrinoless double beta decay process in left-right symmetric models without scalar bidoublet, Phys.Rev., 1, D87, 015002, 10.1103/PhysRevD.87.015002, 2013, 1212.0612

[17] Chakrabortty, Joydeep and Devi, H. Zeen and Goswami, Srubabati and Patra, Sudhanwa, Neutrinoless double-β decay in TeV scale Left-Right symmetric models, JHEP, 08, 2012, 008, 10.1007/JHEP08(2012)008, 1204.2527

[18] Ge, Shao-Feng and Rodejohann, Werner, JUNO and Neutrinoless Double Beta Decay, 2015, 1507.05514

[19] Bhupal Dev, P.S. and Goswami, Srubabati and Mitra, Manimala and Rodejohann, Werner, Constraining Neutrino Mass from Neutrinoless Double Beta Decay, Phys.Rev., D88, 091301, 10.1103/PhysRevD.88.091301, 2013, 1305.0056, MAN-HEP-2013-08, IPPP-13-26, DCPT-13-52

[20] Barry, James and Rodejohann, Werner, Lepton number and flavour violation in TeV-scale left-right

symmetric theories with large left-right mixing, JHEP, 1309, 153, 10.1007/JHEP09(2013)153, 2013, 1303.6324

[21] Nemevsek, Miha and Nesti, Fabrizio and Senjanovic, Goran and Zhang, Yue, First Limits on Left-Right Symmetry Scale from LHC Data, Phys. Rev., D83, 2011, 115014, 10.1103/PhysRevD.83.115014, 1103.1627

[22] Tello, Vladimir and Nemevsek, Miha and Nesti, Fabrizio and Senjanovic, Goran and Vissani, Francesco, Left-Right Symmetry: from LHC to Neutrinoless Double Beta Decay, Phys. Rev. Lett., 106, 2011, 151801, 10.1103/PhysRevLett.106.151801, 1011.3522

[23] Bhupal Dev, P. S. and Lee, Chang-Hun and Mohapatra, R. N., Leptogenesis Constraints on the Mass of Right-handed Gauge Bosons, Phys. Rev., D90, 2014, 9, 095012, 10.1103/PhysRevD.90.095012, 1408.2820, MAN-HEP-2014-11, UMD-PP-014-014

[24] Nemevsek, Miha and Nesti, Fabrizio and Senjanović, Goran and Zhang, Yue, First Limits on Left-Right Symmetry Scale from LHC Data, Phys.Rev., D83, 115014, 10.1103/PhysRevD.83.115014, 2011, 1103.1627

[25] Keung, Wai-Yee and Senjanović, Goran, Majorana Neutrinos and the Production of the Right-handed Charged Gauge Boson, Phys.Rev.Lett., 50, 1427, 10.1103/PhysRevLett.50.1427, 1983

[26] Das, S.P. and Deppisch, F.F. and Kittel, O. and Valle, J.W.F., Heavy Neutrinos and Lepton Flavour Violation in Left-Right Symmetric Models at the LHC, Phys.Rev., D86, 055006, 10.1103/PhysRevD.86.055006, 2012, 1206.0256, IFIC-12-17

[27] Bertolini, Stefano and Maiezza, Alessio and Nesti, Fabrizio, Present and Future K and B Meson Mixing Constraints on TeV Scale Left-Right Symmetry, Phys.Rev., D89, 095028, 10.1103/PhysRevD.89.095028, 2014, 1403.7112

[28] Beall, G. and Bander, Myron and Soni, A., Constraint on the Mass Scale of a Left-Right Symmetric Electroweak Theory from the K_L–K_S Mass Difference, Phys.Rev.Lett., 48, 848, 10.1103/PhysRevLett.48.848, 1982

[29] de Salas, P. F. and Forero, D. V. and Ternes, C. A. and Tortola, M. and Valle, J. W. F., Status of neutrino oscillations 2018: 3σ hint for normal mass ordering and improved CP sensitivity, Phys. Lett., B782, 2018, 633-640, 10.1016/j.physletb.2018.06.019, 1708.01186

[30] Esteban, Ivan and Gonzalez-Garcia, M. C. and Maltoni, Michele and Martinez-Soler, Ivan and Salvado, Jordi, Updated constraints on non-standard interactions from global analysis of oscillation data, Journal of High Energy Physics, Aug 28, 2018, 8, 180, 10.1007/JHEP08(2018)180

[31] Aghanim, N. and others, Planck 2018 results. VI. Cosmological parameters, Planck, 2018, 1807.06209

[32] Ge, Shao-Feng and Lindner, Manfred and Patra, Sudhanwa, New physics effects on neutrinoless double beta decay from right-handed current, JHEP, 10, 2015, 077, 10.1007/JHEP10(2015)077, 1508.07286

[33] "Natural" left-right symmetry, Mohapatra, R. N. and Pati, J. C., Phys. Rev. D, 11, 9, 2558–2561, 0, 1975, May, American Physical Society, 10.1103/PhysRevD.11.2558

[34] Exact left-right symmetry and spontaneous violation of parity, Senjanovic, G. and Mohapatra, R. N., Phys. Rev. D, 12, 5, 1502–1505, 0, 1975, Sep, American Physical Society, 10.1103/PhysRevD.12.1502

[35] Neutrino Mass and Spontaneous Parity Nonconservation, Mohapatra, Rabindra N. and Senjanović, Goran, Phys. Rev. Lett., 44, 14, 912–915, 0, 1980, Apr, American Physical Society, 10.1103/PhysRevLett.44.912

[36] Neutrino masses and mixings in gauge models with spontaneous parity violation, Mohapatra, Rabindra N. and Senjanović, Goran, Phys. Rev. D, 23, 1, 165–180, 0, 1981, Jan, American Physical Society,

10.1103/PhysRevD.23.165

[37] Left-Right Symmetry: From the LHC to Neutrinoless Double Beta Decay, Tello, Vladimir and Nemevšek, Miha and Nesti, Fabrizio and Senjanović, Goran and Vissani, Francesco, Phys. Rev. Lett., 106, 15, 151801, 4, 2011, Apr, American Physical Society, 10.1103/PhysRevLett.106.151801

[38] Pritimita, Prativa and Dash, Nitali and Patra, Sudhanwa, Neutrinoless Double Beta Decay in LRSM with Natural Type-II seesaw Dominance, JHEP, 10, 2016, 147, 10.1007/JHEP10(2016)147, 1607.07655

[39] Search for Majorana Neutrinos Near the Inverted Mass Hierarchy Region with KamLAND-Zen, Gando et al, A., KamLAND-Zen Collaboration, Phys. Rev. Lett., 117, 8, 082503, 6, 2016, Aug, American Physical Society, 10.1103/PhysRevLett.117.082503

[40] Improved Limit on Neutrinoless Double-β Decay of ^{76}Ge from GERDA Phase II, Agostini et al, M., GERDA Collaboration, Phys. Rev. Lett., 120, 13, 132503, 5, 2018, Mar, American Physical Society, 10.1103/PhysRevLett.120.132503

[41] First Results from CUORE: A Search for Lepton Number Violation via $0\nu\beta\beta$ Decay of ^{130}Te, Alduino et al, C., CUORE Collaboration, Phys. Rev. Lett., 120, 13, 132501, 8, 2018, Mar, American Physical Society, 10.1103/PhysRevLett.120.132501

[42] Can nonstandard interactions jeopardize the hierarchy sensitivity of DUNE?, Deepthi, K. N. and Goswami, Srubabati and Nath, Newton, Phys. Rev. D, 96, 7, 075023, 6, 2017, Oct, American Physical Society, 10.1103/PhysRevD.96.075023

[43] Bakhti, Pouya and Farzan, Yasaman, CP-violation and non-standard interactions at the MOMENT, Journal of High Energy Physics, 2016, 7, 109, 1029-8479

[44] de Gouvea, Andre and Friedland, Alexander and Murayama, Hitoshi, The Dark side of the solar neutrino parameter space, Phys. Lett., B490, 2000, 125-130, 10.1016/S0370-2693(00)00989-8, hep-ph/0002064, UCB-PTH-00-03, LBNL-45023, LBL-45023

[45] Review of Particle Physics, Tanabashi et al, M., Particle Data Group, Phys. Rev. D, 98, 3, 030001, 1898, 2018, Aug, American Physical Society, 10.1103/PhysRevD.98.030001

[46] Improved Limit on Neutrinoless Double-β Decay of ^{76}Ge from GERDA Phase II, Agostini et al, M. , GERDA Collaboration, Phys. Rev. Lett., 120, 13, 132503, 5, 2018, Mar, American Physical Society, 10.1103/PhysRevLett.120.132503

Getting Started With Quantum Computation: Experiencing The Quantum Experience

Ranveer Kumar Singh[1], Prathamesh Ratnaparkhi[2], Bikash K. Behera[3] and Prasanta K. Panigrahi[3]**

[1]BS-MS Student, Department of Mathematics, Indian Institute of Science Education and Research Bhopal, Bhauri 462066, Madhya Pradesh, India

[2]Mechanical Engineering, Vishwakarma Institute of Technology, 666, Upper Indira Nagar, Bibwewadi, Pune, Maharashtra 411037

[3]Indian Institute of Science Education and Research, Kolkata, Mohanpur 741246, West Bengal, India

Abstract. Quantum computation is an emerging field of research at the intersection of computer science, information theory and quantum physics. With applications in cryptography, simulation of complex quantum mechanical systems, artificial intelligence, weather forecast and market prediction, quantum computers will be indispensable in the future. Recent years have seen immense progress on the experimental front, with the IBM Quantum Experience (IBM QE), real quantum computers are within reach for anyone. We introduce here the basic concepts of quantum computation for using IBM QE, needing only the knowledge of matrix multiplication.

Keywords. IBM Quantum Experience, Quantum Computation, Superposition, Entanglement

INTRODUCTION

Using principles of quantum physics developed in the early 20^{th} century, a completely new field, "quantum computation" has emerged, unifying computer science, information theory and physics. It started with Richard Feynman's observation [1] that a computer can be designed that can use the laws of quantum mechanics to simulate the nature. The idea was to use a quantum state as the fundamental building blocks of the computer, the simplest one is a two-level system, called a *qubit*, which evolves according to the laws of quantum mechanics. An example of a quantum two-level system can be the two-spin states of an electron or the two polarizations of light. The classical bits are represented by 0 or 1, or physically they can be voltage on and off in a chip. These numbers are manipulated using normal addition operation. Unlike the classical bit that represents only one state at a time, a quantum bit (qubit) can be in both the states at the same time i.e., in a superposition of both the states. As is well-known, "quantum mechanics" also called 'matrix mechanics', a single qubit state is represented by a 2×1 matrix, being a linear superposition of $|0\rangle = [1, 0]^T$ and $|1\rangle = [0, 1]^T$, i.e., $\alpha|0\rangle + \beta|1\rangle$, where $|\alpha|^2 + |\beta|^2 = 1$ and α, β are complex numbers. This superposition of states observed in quantum physics gives an infinitude of states in which a qubit can be, which in turn

** pprasanta@iiserkol.ac.in

increases the computing power of quantum computers. This feature of quantum computers, known as "quantum parallelism" enables us to perform large number of operations in small time interval that reduces the complexity of the problems. Thus classically intractable problems like the travelling salesman problem can be solved on a quantum computer efficiently [2].

More generally, there is a certain class of problems called non-polynomial (NP) problems [3], which cannot be solved efficiently on the current "classical" computers. The phrase "cannot be solved efficiently" means that as the size of the input parameter increases, the time required to solve the problem increases exponentially. Consider the aforementioned travelling salesman problem [4, 5]; a salesman has to visit n different cities, which path should he follow so that he can visit all the cities with the minimum distance travelled? It has been calculated that for number of cities as small as 10 there are 10!/2 =1814400 possible paths in which he can visit them. For solving this problem, a classical computer works in the following way; it will systematically calculate the total distance for each possible configuration and then compare among them to find the optimal solution, i.e., the minimum path among all the possible paths. The time required to solve this problem increases exponentially with the number of cities, thus for a sufficiently large number of cities the computer will take forever to find the solution. Like this, there are other hard problems [6] which require a computer that can perform a large number of operations with minimum time-complexity. This is exactly what a quantum computer can do.

Apart from "quantum parallelism", another peculiar feature which quantum mechanics exhibits is *Entanglement* [7]. Entanglement refers to two or more quantum particles having correlated quantum states. For example, in a singlet state, two electrons are physically separated and in anti-parallel directions. The quantum state of the two electrons can be written as, $\frac{|01\rangle - |10\rangle}{\sqrt{2}}$, where $|0\rangle$ and $|1\rangle$ stand for spin-up and spin-down states of electrons. Entanglement allows to perform an operation on two qubits simultaneously which cannot be done with classical bits. Thus qubits can exist in superposition of more than one state and also can be entangled with each other, which classical bits cannot exhibit. Using these features of quantum mechanics, several non trivial algorithms have been designed in quantum computation. Quantum teleportation [8], where an unknown quantum state is transferred between two distant parties, has been achieved using entangled channels (Sec. 3) between the sender and the receiver.

There are ways to improve the efficiency of classical computers. For instance, one way would be to make bigger computers i.e., to have more transistors on a chip. A bigger computer solves a problem of given size in less time. In order to tackle problems of bigger and bigger size in less and less time, the transistors will have to get smaller and smaller, so small that eventually there are only a few silicon atoms. According to Moore's law [9], "The number of transistors in a dense integrated circuit doubles every two years". At this stage, we again fall prey to the laws of quantum physics due to the small size. Heat generation in the computing process is another disadvantage working in the microscopic level. In Landauer's principle [10], it is argued that "a minimum heat generation, of the order of κT, is required for each irreversible function". Thus the emergence of quantum computers under a well defined framework of quantum mechanics has been one of the most

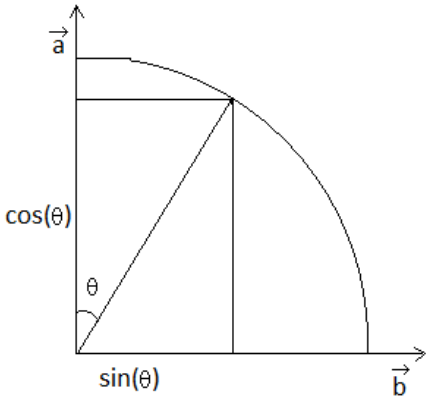

Figure 1. The state of a polarized light

important developments of the 20^{th} century.

1. ORIGIN OF RANDOMNESS

Superposition is at the heart of quantum computation since it gives rise to randomness. To understand how randomness comes up at microscopic scale, consider an example of plane polarized light incident on a polarizer. If we represent the state of polarization parallel to optical axis by $\vec{a}$ and the state perpendicular to it by $\vec{b}$ then a photon polarized at an angle θ with respect to the vertical axis can be represented as $\vec{x}(\theta) = (\vec{x}(\theta) \cdot \vec{a})\vec{a} + (\vec{x}(\theta) \cdot \vec{b})\vec{b} = (\cos\theta)\vec{a} + (\sin\theta)\vec{b}$. Fig. 1 illustrates this fact. When light with this state of polarization $\vec{x}(\theta)$ travelling along z axis, is incident on a polarizer it is observed that transmitted intensity is $\cos^2(\theta)I_0$, where I_0 is incident intensity and θ is angle between plane of polarization and optical axis.

Now suppose we have some kind of an apparatus which emits only one photon at a time. Then if using the apparatus we let a photon strike the polarizer then the photon will either pass through or it will be absorbed. What decides whether the photon will pass through polarizer or not? Passing photon through polarizer constitutes a measurement and according to Copenhagen interpretation of quantum mechanics the state of the system collapses to one of the basis states upon measurement. This collapse is totally random and all we can talk about a priory is the probability with which the photon will collapse to given basis state. An analogy of coin toss will be helpful to understand the idea of superposition-measurement-collapse. When the coin is in air it is neither heads nor tails, it is in superposition. As it hits the ground it lands on heads or tails at random. The probability that an incident photon in state $(\cos\theta)\vec{a} + (\sin\theta)\vec{b}$ will collapse to state $\vec{a}$ is given by $\cos^2(\theta)$ and that of state $\vec{b}$ is $\sin^2(\theta)$. Note that the sum of probabilities i.e., $\sin^2(\theta)+\cos^2(\theta)$ is 1. Thus out of n incident photons $\cos^2(\theta).n$ are randomly found in state $\vec{a}$ and thus the transmitted intensity is $\cos^2(\theta)I_0$. This analysis at microscopic scale is totally consistent with macroscopic intensity law (Malus' Law). If

we rotate the analyzer such that the optical axis is parallel to the plane of polarization (rotation of measurement basis) then the photon is in state $\vec{a}$. Now $\cos^2(\theta) = 1$, thus every photon that arrives at polarizer passes through. There is no random behaviour. We see that randomness arises when the system is in superposition of measurement basis states.

2. THE POWER OF SUPERPOSITION

Interestingly, the same superposition which leads to randomness also allows for performing operations on all possible states at once. This leads to quantum parallelization i.e. unlike classical computer which has to process one input at a time a computer based on quantum principles, a "Quantum Computer" can process all possible inputs at once. Quantum parallelization relies on the fact that a qubit can exist in a superposition of base states. Each component of this superposition can be thought of as a single argument of a function. A function operated on the qubit, which is in a superposition of states, is thus operated on each of the components of the superposition, but this function is only applied one time. Since for n qubits, there are a total of 2^n possible states, thus what would take a classical computer an exponential number of operations, can be performed on a quantum computer in one operation. Although quantum parallelization offers a large speedup over classical computers, the result may still be random, so the whole idea is to design the operations in such a way that the probability of getting the correct answer is enhanced. But this has its own shortcomings. With larger number of superposed states, the probability of measuring a particular superposed state becomes low and hence the answer is probabilistic. Moreover, according to the laws of quantum mechanics, superposition is lost upon measurement on the quantum state. Thus if we only use superposition states then the probability of retrieving the answer is low. But for problems which are beyond reach of classical computers a probabilistic answer is better than no answer at all. Fortunately in some cases, although the solution is difficult to find, it is easy to check a given solution. For example, finding out prime factors of a number is a NP hard problem [3], but given a prime factor of a number it is just matter of easy multiplication to check whether they are really the prime factors or not. Thus a parallel computing algorithm can be devised to multiply all the factors in just one operation. Thus a probabilistic answer can be checked and if found incorrect, the process can be rerun to find another answer.

3. QUANTUM ENTANGLEMENT

Quantum entanglement as introduced earlier is the distinguishing feature of quantum mechanics. In mathematical language, a two qubit state can be represented as,

$$|\psi\rangle = \Big(a|0\rangle + b|1\rangle\Big) \otimes \Big(\alpha|0\rangle + \beta|1\rangle\Big) = a\alpha|00\rangle + a\beta|01\rangle + b\alpha|10\rangle + b\beta|11\rangle \qquad (1)$$

where $\otimes$ is the tensor product between the two quantum states, and $|00\rangle = |0\rangle \otimes |0\rangle$, similarly it applies for other states, $|01\rangle$, $|10\rangle$, and $|11\rangle$. The above state (Eq. (1)) reveals that the first qubit is

in the state $a|0\rangle + b|1\rangle$ and the second qubit is in the state $\alpha|0\rangle + \beta|1\rangle$. Now consider another such state:

$$|\psi\rangle = \frac{1}{\sqrt{2}}(|01\rangle - |10\rangle) \tag{2}$$

It is an easy exercise to check that this state cannot be factored in the form $(a|0\rangle + b|1\rangle)(\alpha|0\rangle + \beta|1\rangle)$. Hence it shows that the state of individual qubits are not completely specified. States of the form Eq. (2) are called entangled states. The state in Eq. (2) is called EPR pair after Einstein, Podolsky and Rosen [11] who used this state to propose a paradox in quantum mechanics (famously known as EPR paradox). This state has the property that measurement on one of the qubit reveals the state of the other instantaneously. Such states are of utmost importance in quantum computation. As discussed above we observe that measurement on one qubit of an entangled state determines the state of the other irrespective of their location in space. Thus entangled states have been used as communication channel in cryptographic protocols. All of quantum key distribution (QKD) protocols which provide a way to share a private key between two parties (Alice and Bob) separated in space, rely on entanglement. These protocols use entanglement to check if a key sent by one party has been hijacked in between by eavesdropper. In most of the QKD protocols, if Alice wants to send a secret key to Bob then firstly they prepare some entangled state with each of them having half of the entangled particles. Then Alice performs a measurement on some of her particles and then communicates the result to Bob via classical channel. Since immediately after the measurement the state of the other half of the particles is known to Bob as communicated by Alice, he measures his particles to check if someone has tried to access the key by measuring on his particles. If Bob finds the same result as informed by Alice then he can be sure that the key shared is secret. Some modifications of this protocol is used in most of these protocols. It is also known that Grover's search algorithm and Shor's factorization algorithm, which are some of the most important quantum algorithms use entangled states [12, 13].

4. QUANTUM COMPUTER

Quantum computers are built from *quantum circuits* which consist of wires and elementary *quantum gates*, in the same fashion as classical computers are made using electrical wires and logic gates. Quantum gates are used to carry around and manipulate quantum information encoded in qubits. In the language of quantum mechanics a qubit is represented by the superposition state $\alpha|0\rangle + \beta|1\rangle$ where $|0\rangle$ and $|1\rangle$ are the two states of a quantum bit analogous to the 0 and 1 state of a classical bit (cbit). A qubit can be physically represented by trapped ions, superconducting junctions, NMR etc. Quantum gates are the implementation of operations performed on a quantum state by Linear operators. In the language of mathematics we say that quantum states are vectors in a mathematical object called Hilbert space. Thus the mathematical language of quantum mechanics is Linear algebra. The operators acting on quantum states are represented by matrices. So any manipulation of a quantum

state is carried out by operators. In quantum computation, these operations are realized via quantum gates. There are several quantum gates classified as single qubit gate and multiple qubit gate which as the names suggest act on single qubit and multiple qubits respectively. Thus a quantum computer essentially consists of a series of qubits, each of which is a quantum system described using two dimensional vector space. The qubits are prepared in known state say, $|0\rangle$ then a transformation is applied on them which puts them in superposition. Once in superposition a series of transformations via quantum gates are applied which act on every possible input. After quantum gates act on the qubits, a measurement is done to retrieve the answer. Using this procedure different quantum algorithms are designed to solve various problems using quantum circuits constructed using a specified sequence of quantum gates.

5. A BRIEF HISTORY OF QUANTUM COMPUTATION

In the 1920s, with the evolution of quantum mechanics which had already resolved several absurdities such as "ultraviolet catastrophe" and the instability of atom due to electron's accelerated motion etc predicted by classical physics, people started to think if quantum mechanics could be used to achieve things which classically cannot be achieved. For example in the early 1980s, researchers started thinking if quantum effects could be used to signal faster than light which was forbidden classically according to the special theory of relativity. It turned out that this problem was equivalent to cloning a quantum state which is very well possible classically. However, it was proved that it was impossible to clone a quantum state [14]. This *no-cloning theorem* was one of the earliest results in quantum computation and quantum information. Making use of this no-cloning theorem, the first idea in the field of quantum information called "Quantum Money" was proposed by Stephen Wiesner in 1970 (which remained unpublished until 1983) [15].

In 1981 Richard Feynman had realized that the inability of computers to simulate quantum mechanical systems is because their working principles are classical. He proposed that a computer used for simulation of quantum mechanical systems should be based on quantum principles. To use quantum principles for computing, it was necessary to gain complete control over quantum state which is so fragile towards environmental effects. Thus since 1970s many such techniques were developed. For example, methods were developed to trap a single atom in an "atom trap" and study its properties with stunning accuracy. In the mean time computer science was also developing rapidly with the remarkable paper by Alan Turing in 1936 [16]. Turing presented a notion of what we call a programmable, a model for computation called *Turing machine*. Subsequently, John Von Neumann developed a theoretical model to build a practical computer which would be capable as a *Universal Turing machine*. In the late 1960s, the *Church Turing* thesis was presented, which states that "Any algorithmic process can be simulated efficiently using a Turing machine". However, the challenge came when it was observed that many problems which were believed to have no solution on Turing machine could be solved using *analog computers*. But the problem was that if the realistic assumptions of noise in analog computers were taken into account, then it was difficult to operate

on such problems. This challenge was successfully resolved when the theory of *error correcting codes* and *fault tolerant quantum computation* was proposed. Following this several quantum algorithms were proposed to solve various problems. From late 60s to late 90s the research in the field led to formation of theoretical framework for quantum information. The most important of them, the *factorization algorithm* by Shor (1994) [17] and *list search algorithm* by Grover (1996) [18] demonstrated the power of quantum computation. The first experimental demonstration of quantum algorithm was done in 1998 by Jones and Mosca at Oxford University [19].
Since late 1990s, experimental side has progressed tremendously. Linear optics, superconducting junction, nuclear magnetic resonance and trapped ions have been used as qubits. However, efforts to build quantum computers have not met great successes till date. Small quantum computers capable of performing dozens of calculations on a few qbits have been developed but the problem of building a universal quantum computer still remains a challenge for future researchers. A huge step in the development of a universal quantum computer has been accomplished by IBM [20], which has developed 5-, 16-, 20- and 50-qubit quantum computers. Two of them, the 5- and 16-qubit quantum computers are available to public, providing an opportunity to everyone to perform experiments on the quantum computers.

6. IBM Q EXPERIENCE

With continuous efforts, IBM developed a quantum computer which used superconducting qubits. Since its inception in May 2016, IBM Quantum Experience (IBM QE) has proven to be a valuable asset for researchers working in the field of quantum computation. More than 80 academic papers have been published based on the research carried out with help of IBM QE. Through this platform, researchers, students and enthusiasts get access to a real quantum processor and a simulator. The qubits used are superconducting Josephson junctions. They are stored at very low temperature, only a few miliKelvin above absolute zero, in order to protect them from the thermal noise. A $^3He/^4He$ dilution refrigerator is used to achieve the required low temperature. The state of a qubit is changed by shooting it with microwave radiation of predetermined frequency and phase. On the other hand, measurement of the state of a qubit is done by measuring its response to certain microwave radiation.

As of November 2018, IBM has made available two 5-qubit and one 16-qubit quantum computers. These devices can be remotely accessed using Quantum Information and Science Kit (QISKit) provided by IBM QE. The quantum composer (Fig. 2) is a user friendly graphic user interface developed by IBM, used to write quantum algorithms or run experiments in the field of quantum computation and quantum information. Along with composer, the online platform includes a beginner's guide, a full user's guide and a forum to share ideas and reach out for help. The typical process of writing and running an algorithm is as follows: initially, all the qubits in composer are in the state $|0\rangle$, appropriate gates are taken from side panel and dropped on a qubit to change the state of the qubit. The information processing occurs when the state of one qubit is conditionally evolved based on the state of some other qubits using conditional gates (e.g. $CNOT$ gate). Finally measurements

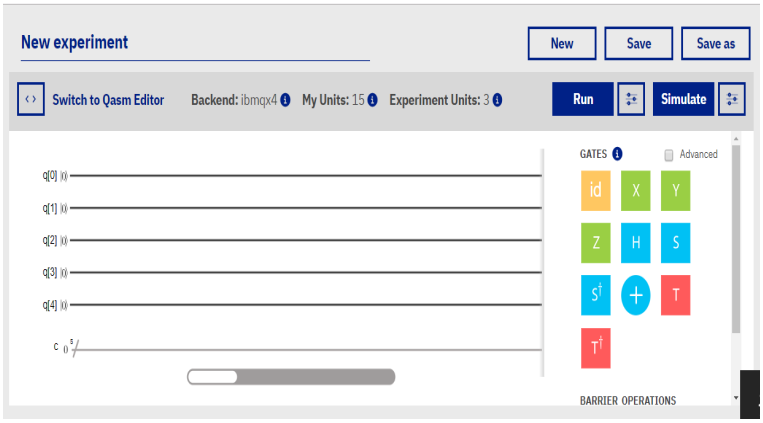

Figure 2. The composer of IBM Q Experience. Image Credit:IBM Q Experience.

are done to know the states of all or some qubits and the results are stored in classical registers and displayed as a bar chart. For example, a two-qubit algorithm can have four possible outcomes $|00\rangle$, $|01\rangle$, $|10\rangle$ and $|11\rangle$. So the result of a two-qubit algorithm gives probability of getting each one of these as output. As we know for a particular run, the result is random but when we run the algorithm many times we may find that a certain result occurs more often than other. The whole idea is to apply transformations (quantum gates) in such a way that the probability of getting desired output is enhanced.

To start building quantum circuits one first needs to visit IBM QE website and register with email addresses. Then go to the composer and start a new circuit. There is an option to choose to run the circuit on real quantum computer or simulate the results using custom topology. A circuit sent to run on the real device, is queued and the process takes time. Thus it is advisable to use custom topology for trial and error and for testing the circuit prior to sending it to real device. Quantum algorithms involving 5 qubits can be constructed using the quantum composer but implementing a 16 qubit algorithm requires writing the algorithm in QASM language. Then it can be run on the real quantum computer or simulated using QISKit. It is to be noted that QISKit is an open-source framework for working with noisy quantum computers at the level of pulses, circuits, and algorithms.

Thus running a real time quantum computer is now at hand. Observing bizarre quantum phenomena such as quantum teleportation, cryptography protocols can be easily realized on IBM Q. IBM Q is improving the quantum computing power day by day. IBM Q has recently announced a 50-qubit quantum computer for commercial purposes. A number of experiments in the field of quantum computational and information processing have been performed on the 5-qubit, and 16-qubit real quantum chips. Experimental realization of quantum cheque [21–23], observation of Topological Uhlmann phase [24], algorithmic simulation [25], developing quantum error correction codes [26–29], experimental test of Mermin's inequalities [30], testing quantum algorithms [31], optimization of quantum circuits [32] etc. have been tested and verified on the real quantum chips.

7. CONCLUSION

We have seen that a paradigm shift from classical to quantum computation allows us to solve classically intractable problems which could not be solved efficiently before. In brief, we have tried to motivate young students to experiment in the field of quantum computation, using the publicly available quantum computers. Furthermore, quantum computers of different architecture and a brief history of quantum computation have been discussed. The IBM QE platform has been discussed, which anyone can use and implement protocols on a real quantum computer. There are a number of problems for which quantum algorithms are yet to be designed. With the help of IBM QE, any interested researchers can participate in the effort to take the research in quantum computation forward.

References

[1] R. P. Feynman, *Int. J. Theor. Phys.*, Vol. 21, pp. 6-7, 1982.

[2] S. Aaronson, *Quantum Computing Since Democritus*, Cambridge University Press, 2013.

[3] M. A. Nielsen and I. L. Chuang, *Quantum Computation And Quantum Information*, Cambridge University Press, 2010.

[4] D. C. M. Jose,*Transportation Research Part*, Vol. 33, pp. 123-152, 1999.

[5] K. Srinivasan, S. Satyajit, B. K. Behera, and P. K. Panigrahi, *arXiv:1805.10928*, 2018.

[6] D. P. Bovet, *Introduction to the Theory of Complexity*, Prentice Hall, 2006.

[7] E. Schrodinger, *Naturwiss.*, Vol. 23, p. 807, 1935.

[8] C. H. Bennett, G. Brassard, C. Crepeau, R. Jozsa, A. Peres, and W. Wootters, *Phys. Rev. Lett.*, Vol. 70, p. 1895, 1993.

[9] G. E.Moore, *Electronics*, Vol. 38, p. 8, 1965.

[10] R. Landauer, *IBM J. Res. Develop.*, Vol. 5, pp. 183-191, 1961.

[11] A. Einstein, B. Podolsky, and N. Rosen, *Phys. Rev.*, Vol. 47, p. 777, 1935.

[12] V. M Kendon, *Quantum Inf. & Comput.*, Vol. 6, pp. 630-640, 2006.

[13] S. Chakraborty, *arXiv:1305.4454v2*, 2013.

[14] W. K. Wootters and W. H. Zurek, *Nature*, Vol. 299, pp. 802-803, 1982.

[15] S. J. Wiesner, *SIGACT News*, Vol. 15, pp. 78-88, 1983.

[16] A. M. Turing, *Proceedings of the London Mathematical Society*, Vol. s2-42, pp. 230-265, 1937.

[17] L. M. K. Vandersypen, M. Steffen, G. Breyta, C. S. Yannoni, M. H. Sherwood and I. L. Chuang, *Nature*, Vol. 414, pp. 883-887, 2001.

[18] L. K. Grover, *Proceeding STOC '96 Proceedings of the twenty-eighth annual ACM symposium on Theory of computing*, pp. 212-219, 1996.

[19] J. A. Jones and M. Mosca, *J. Chem. Phys.*, Vol. 109, p. 1648, 1998.

[20] IBM Quantum Experience, URL: https://quantumexperience.ng.bluemix.net/qx/editor.

[21] S. R. Moulick and P. K. Panigrahi, *Quantum Inf. Process.*, Vol. 15, pp. 2475-2486, 2016.

[22] B. K. Behera, and A. Banerjee, and P. K. Panigrahi, *Quantum Inf. Process.*, Vol. 16, p. 312, 2017.

[23] News in New Scientist, *URL: https://www.newscientist.com/article/2140242-quantum-cheques-could-be-a-forgery-free-way-to-move-money/.*

[24] O. Viyuela, A. Rivas, S. Gasparinetti, A. Wallraff, S. Filipp, and M. A. Martin-Delgado, *npj Quantum Inf.*, Vol. 4, p. 10, 2018.

[25] A. A. Zhukov, S. V. Remizov, W. V. Pogosov, and Y. E. Lozovik, *Quantum Inf. Process.*, Vol. 17, p. 223, 2018.

[26] C. Vuillot, *Quantum Inf. Comput.*, Vol. 18, p. 0949, 2018.

[27] D. Ghosh, P. Agarwal, P. Pandey, B. K. Behera, and P. K. Panigrahi, *Quantum Inf. Process.*, Vol. 17, p. 153, 2018.

[28] J. R. Wootton and D. Loss, *Phys. Rev. A*, Vol. 97, p. 052313, 2018.

[29] S. Satyajit, K. Srinivasan, B. K. Behera, and P. K. Panigrahi, *Quantum Inf. Process.*, Vol. 17, p. 212, 2018.

[30] D. Alsina and J. I. Latorre, *Phys. Rev. A*, 94, p. 012314, 2016.

[31] S. Gangopadhyay, Manabputra, B. K. Behera, and P. K. Panigrahi, *Quantum Inf. Process.*, Vol. 17, p. 160, 2018.

[32] M. Sisodia, A. Shukla, A. A. A. de Almeida, G. W. Dueck, and A Pathak, *arXiv:1812.11602*, 2019.

Mirage in geometrical optics and the horizontal ray

Dhiman Biswas[1] [*], **Simran Chourasia**[2] [†], **Rathindra Nath Das**[1] [‡], **Rajesh B. Khaparde**[3] [§], **Ajit M. Srivastava**[4] [¶]

1. B.Sc. final year, Ramakrishna Mission Residential College Narendrapur, Kolkata - 700103
2. M.Sc. 3rd year, National Institute of Science Education and Research, Bhubaneswar
3. Homi Bhabha Centre for Science Education, TIFR, Mankhurd, MUMBAI – 400088
4. Institute of Physics, Bhubaneswar 751005

Abstract. Mirage forms when light rays traversing a medium with spatially varying refractive index bend and undergo total internal reflection. Typical example is when downward going light rays bend upward when heated air in contact with hot earth surface leads to vertical gradient of refractive index with refractive index increasing in upward direction. A conceptual issue arises when considering the part of the light trajectory where light ray becomes horizontal. With refractive index varying only in the vertical direction, one will expect from symmetry considerations that a horizontal ray should not bend, contrary to the observed phenomenon of mirage. This issue has been discussed in literature, e.g. by Raman and Pancharatnam and by Berry. We discuss their arguments and argue that there are subtle conceptual issues in understanding mirage strictly in the framework of geometrical optics. In particular, we consider a horizontally moving light ray and argue that within geometrical optics, such a ray should continue to move horizontally. Bending of such a ray, as required by the mirage phenomenon, must require considerations of wave nature of light.

Keywords: Mirage, geometrical optics, wave optics, Fermat's principle, horizontal ray

1. INTRODUCTION

Nature is full of beautiful optical phenomena and mirage is undoubtedly one of the most interesting one of those. Mirage has been studied for a long time from the aspect of wave and ray optics but still there remain confusions about the bending of light while traveling in a medium with gradient in refractive index. This problem has been addressed by many scientists and a good details of the literature is available in Berry's paper [1] where he has analyzed subtleties of this issue. The popular explanation of mirage in the context of geometric ray considers medium as composed of thin layers with refractive index fixed in each layer and gradually varying with height. We consider a ray making a certain angle of incidence with the plane of stratification and then the ray continues to proceed through the layers from denser to lighter medium and hence changing the angle of incidence.

[*] e-mail:biswasdhiman44@gmail.com
[†] simran.chourasia@niser.ac.in
[‡] rdasph@gmail.com
[§] rajesh@hbcse.tifr.res.in
[¶] ajit@iopb.res.in

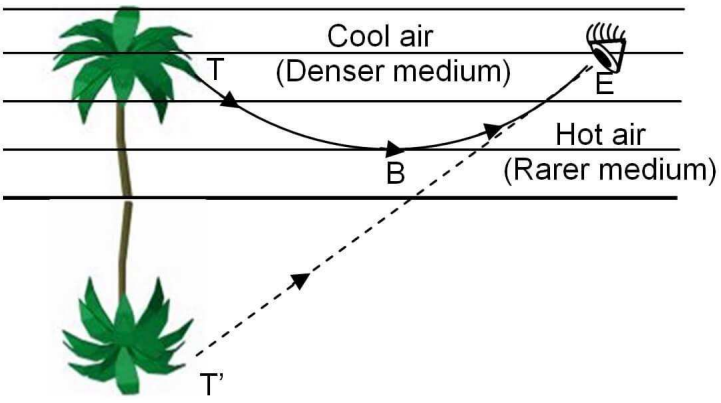

Figure 1. Trajectory of light in mirage

Finally the angle of incidence crosses the critical angle between two successive layers and at that point the light ray undergoes total internal reflection which results in the bending of light towards the denser medium, thereby forming the mirage.

However, this simple sounding explanation ignores underlying questions and subtleties. There are certain parts of this argument which lead to conceptual problems. As the refractive index changes continuously in the vertical direction, the change of incident angle in each (hypothetical) layer will be infinitesimally small. As the ray bends upward continuously, there must be a point where the light ray becomes horizontal. The importance of this *horizontal ray* was discussed by Raman and Pancharatnam [2] and later by Raman [3]. They argued that while continuously bending upward, the light ray should become horizontal (see Figure 1) after successive refractions and then it would not face any change in refractive index in the medium and it should move in a straight line. Basically, the argument relies on symmetry consideration. In geometrical optics, a single light ray is a thin light beam (of thickness approaching zero). Such a ray traversing a medium horizontally where refractive index is constant in horizontal plane should have no reason to change its direction. Note that this argument of symmetry fails if we consider light as a wave since a wave of finite wavelength will necessarily sense vertical gradient of refractive index thereby violating considerations solely relying on horizontal symmetry.

We will discuss the standard approach of explaining mirage in geometrical optics using the laws of reflection and refraction which can be derived, e.g. using Fermat's principle. A light ray traveling from a denser to a lighter medium, with critical incident angle leads to a horizontal (parallel to the interface between the two media) refracted ray. As Fermat's principle is simply a statement of extremal time taken by a light ray between two points, it must respect time reversal symmetry. It then implies that a light ray traveling horizontally (parallel to the interface) will bend towards denser medium, thereby resolving the confusion about the fate of horizontal ray as needed for the mirage phenomenon. However, it should be noted that geometrical optics (hence the use of Fer-

mat's principle) only has the information about direction of reflected and refracted rays, and any information about the relative intensities of these rays requires the treatment of wave nature of light (e.g. using Fresnel's coefficients with the information about the polarization of the light etc.). For example, a complete treatment of reflection and refraction at a *sharp* interface between two media using Maxwell's equations shows that when the incident angle of light ray traveling from a denser to a lighter medium approaches the critical value (with the refracted light ray becoming parallel to the interface), the intensity of this refracted ray approaches zero [4]. This is the situation of total internal reflection when the entire intensity of the incident light is contained in the reflected component alone. With this knowledge, one can see that there is no sense in which one can use time reversal argument to conclude that a horizontal light ray should bend towards denser medium, as the horizontal ray which is being time reversed carries no energy. Indeed, Maxwell equations directly show that a horizontal light ray (traveling parallel to a sharp interface) leads to zero intensity for refracted ray, with the entire energy carried by the reflected ray (which continues in the horizontal direction).

We will also discuss arguments of Berry who has addressed the problem of this horizontal ray [1]. It is argued in [1] that the argument in ref.[2] about horizontal ray is not correct due to a peculiar singularity in the equation governing the bending of light ray in a medium with vertically varying refractive index. We will re-visit these discussions and argue that, while the issue of the singularity is indeed non-trivial, the conclusions reached in Berry's paper are also not very clear. We will argue that the standard approach of focusing on refracted ray cannot lead to correct understanding of mirage in the geometrical optics framework. What one needs is that at certain point during the bending trajectory of light, one needs to switch attention to the reflected light (which carries the entire intensity of incident light in that part of the medium), while any refracted light continues with zero intensity. This reflected light then leads to a refracted component which continues bending upward, finally leading the the standard mirage. (It then becomes an interesting problem to check what differences arise in the actual trajectory of light ray, especially near the horizontal segment, when one switches attention to the reflected ray compared to continuing follow up of the transmitted ray via Fermat's principle.)

To have our discussion well defined (and not subject to the non-trivial issue of singularity in the bending equation as discussed in [1]) we will focus our discussion on the light ray which is initially traveling horizontally (parallel to the plane of symmetry of refractive index, which is assumed to vary only in vertical direction). We will then argue that within geometrical optics, this light ray should not bend. This is what one expects from the symmetry of the problem. A ray which is horizontal and is moving in a medium (of thin layer) where the refractive index is constant should not *know* about the change of refractive index in the layers which are above and below of it. We will also recall discussion from [5] where bending of light in medium for the general case with refractive index gradient has been discussed. We will see that the direction of principle normal of a straight line which is used to derive the bending of light ray can not be defined for a horizontal light ray and hence that approach does not work. In fact, if we take a special case of horizontal ray

and follow the same argument then we obtain the result that it should go in a straight line. We will also briefly discuss the derivation by Raman and Pancharatnam [2] using wave nature of light which gives correct explanation of mirage.

A convenient realization of mirage phenomenon generally uses sugar solution in a jar with vertically varying sugar concentration (with higher concentration, hence higher refractive index being in the downward direction). We have used such a setup and performed measurements to check various aspects of the arguments used above. An important measurement for this purpose is the value of $\frac{dn}{dz}$ for which we have followed a method used in literature by Barnard and Ahlborn [6].

The paper is organized in the following manner. In Sect.2, we discuss about the consideration of intensity for the geometric ray approach of light bending in a medium with vertically varying refractive index. We use equations for the intensity of refracted ray obtained from Maxwell equations for the case of a sharp interface separating two media of different refractive indices. We then argue why the application of Fermat's principle for discussing bending of a horizontal ray gives misleading conclusions. In Sect.3 we describe our experiment which we carried out to confirm these conclusions about intensity measurements of refracted ray. In Sect.4, we first present the argument of Raman and Pancharatnam [2] about the issue of bending of horizontal ray in geometrical optics where they conclude that within geometrical optics a horizontal ray should not bend. We then present arguments of Berry [1] who pointed out a peculiar singularity in the equation of bending of light in mirage within geometrical optics thereby concluding that the argument in [2] does not hold. We will discuss the analysis in ref.[1] and argue that the treatment of singularity is not satisfactory. In Sect.5 we start by considering all these different arguments, including the calculations in [5] about bending of light. As we are not able to reach any definite conclusions about the issue of singularity in the general bending equation (as discussed in refs.[1, 5]) for a medium with continuously varying refractive index, we will then focus on a special case of initially horizontal ray. We will analyze the propagation of such a ray in the medium and draw conclusions from all these different approaches. In Sect.6 we give the results of our experiments which we have carried out to measure $\frac{dn}{dz}$ using the method of ref.[6]. In Sect.7, we conclude by referring to the satisfactory wave optics explanation of mirage given by Raman and Pancharatnam [2, 3], and present our conclusions about the problems with the geometrical optics approach. We also point out future experiments/analysis which can be carried out for further understanding this very intriguing issue of the beautiful phenomenon of mirage.

2. CONSIDERATION OF INTENSITY IN GEOMETRICAL OPTICS

When light beam is incident on a sharp interface of two media with different refractive indices, Maxwell's equations give the following expression for reflection coefficient of the incident light (for s-polarized light) [4]:

$$R = |\frac{n_1 \cos\theta_i - n_2 \cos\theta_t}{n_1 \cos\theta_i + n_2 \cos\theta_t}|^2 \tag{1}$$

Consider the case when R = 1, i.e. intensity of transmitted light is zero.

$$R = 1$$
$$\implies (n_1 \cos\theta_i - n_2 \cos\theta_t)^2 = (n_1 \cos\theta_i + n_2 \cos\theta_t)^2$$
$$\implies \cos\theta_i \cos\theta_t = 0$$
$$\implies \text{either } \cos\theta_i = 0 \text{ or } \cos\theta_t = 0$$
$$\implies \text{either } \theta_i = \pi/2 \text{ or } \theta_t = \pi/2$$

(This result also holds for the p-polarized light as in that case the only change in Eq.(1) is that n_1 and n_2 are exchanged.)

Case 1: $\theta_t = \pi/2$

Snell's law gives

$$\theta_i = sin^{-1}(\frac{n_2}{n_1}) \tag{2}$$

Since domain of sin^{-1} is [-1,1], we have $n_2 \leq n_1$ (dense to rare medium)

$$\therefore \theta_i = sin^{-1}(\frac{n_<}{n_>}) = \theta_c = \text{ critical angle (Figure 2)}$$

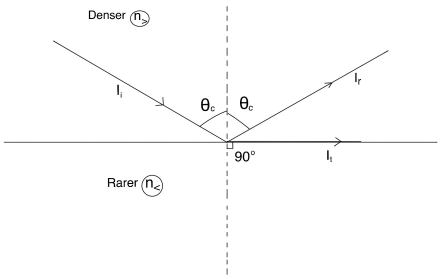

Figure 2. Ray diagram for $\theta_t = \pi/2$

Case 2: $\theta_i = \pi/2$

From Snell's law, $n_1 \sin\theta_i = n_2 \sin\theta_t$

$$\implies \theta_t = sin^{-1}(\frac{n_1}{n_2})$$

Again, with the domain of sin^{-1} is [-1,1], we have $n_1 \leq n_2$ (rare to dense medium)

$$\therefore \theta_t = sin^{-1}(\frac{n_<}{n_>}) = \theta_c = \text{ critical angle (Figure 3)}$$

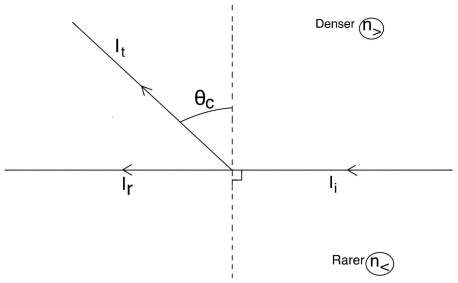

Figure 3. Ray diagram for $\theta_i = \pi/2$

Therefore, horizontal incident light ray with zero intensity (because R=1) bends toward denser medium at angle θ_c. And complete intensity gets reflected at angle 90^o (see Figure 3).

Thus we see that in discrete layer picture of mirage, the bending of light towards the denser layer after the ray becomes horizontal (i.e. tangential to the interface of two layers, with the incident angle $\theta_i = \pi/2$) can be understood in geometrical optics. However, this conclusion holds if we only consider the directions of different rays without any consideration of their respective intensities.

Let us now re-visit the argument about bending of horizontal ray in the framework of geometrical optics. The basic principle of geometrical optics is *Fermat's principle*. It says that to go from one point to another point, any light ray will follow the path in which optical path will be extremum. Using this principle we can derive the basic laws of geometrical optics like *The law of reflection* and *The law of refraction (Snell's law)*. Here our interest lies in the *Law of refraction* which says

$$n_i \sin\theta_i = \text{constant} \tag{3}$$

Here n_i is the refractive index of ith medium and θ_i is the angle of refraction in ith medium.

Now if a light ray is traveling from one medium (say medium 1) to anther medium (say medium 2) the Snell's law reduces to $n_1 \sin\theta_1 = n_2 \sin\theta_2$. But Snell's law only gives us the information of the direction of light ray. It has no information about relative intensities of different rays. This becomes of crucial importance when critical angle is involved. From Snell's law we can see that at critical angle of incidence, the transmitted ray becomes horizontal. But we saw above that Maxwell's equations show that in this case, the transmitted light has zero intensity, i.e. it will not carry any energy. In this condition the total light will be reflected at critical angle which is the case of total internal reflection. Let us continue with this use of Fermat's principle (neglecting considerations of intensity) that a light ray incident at critical angle θ_c $(= sin^{-1}(n_</n_>))$ on a sharp interface from denser to rarer medium gets refracted at angle 90^o. Time reversal symmetry of Fermat's principle implies that a ray incident at 90^o on a sharp interface from rarer to denser medium will get refracted to denser medium at an angle equal to θ_c. This is what underlies the standard explanation of mirage in geometrical optics using Fermat's principle. So at the lowest point of trajectory in mirage, the

ray becomes horizontal (90^o incidence) and gets refracted to the upper denser layer at an angle θ_c corresponding to the concerned two layers.

Now we bring in the consideration of intensities of different rays (Eq.(1)). Case 2 above (for ray propagating from rarer medium to the denser medium with incidence angle $\theta_i = 90^o$) shows that although the ray bends towards in the denser medium at θ_c, it's intensity is zero and the total intensity of light continues in a straight line. Main conclusion one can draw from this discussion is that to have a correct explanation of mirage in discrete layer picture of the medium, one cannot just focus on the transmitted light with the equation $n_i sin\theta_i =$ constant for each successive layer. At some point, when the incident angle equals critical angle between two consecutive layers, the attention must be shifted to the reflected ray with the equation $\theta_i \equiv \theta_{incidence} = \theta_{reflected}$. This takes care of the main puzzle of horizontal ray, in the sense that in discrete layer picture there will simply be no horizontal ray ever having a non-zero intensity. The horizontal transmitted ray will carry zero intensity at the point when one shifts attention to the reflected ray. Subsequently, one can just follow that ray, again focusing on the transmitted ray all along, finally leading to the phenomenon of mirage. Of course, all this holds in the discrete layer picture of the medium and these arguments need to be made rigorous for a medium with continuous variation of refractive index.

In the next section we will describe our experiment which we have carried out to verify the above conclusions about intensities of refracted and reflected rays using Eq.(1).

3. EXPERIMENTAL STUDY OF TRANSMISSION OF LIGHT AT AN INCIDENT ANGLE OF 90^O

In this experiment, relative intensity of reflected light for different angles of incidence is measured for air-water interface and for air-acrylic interface using the apparatus in Figure 4. The experiments were done using solid state red laser whose angle of incidence was measured. Intensity of reflected light was measured using a CCD detector. The heights of the laser source and the detectors could be changed depending on the angle on incidence.

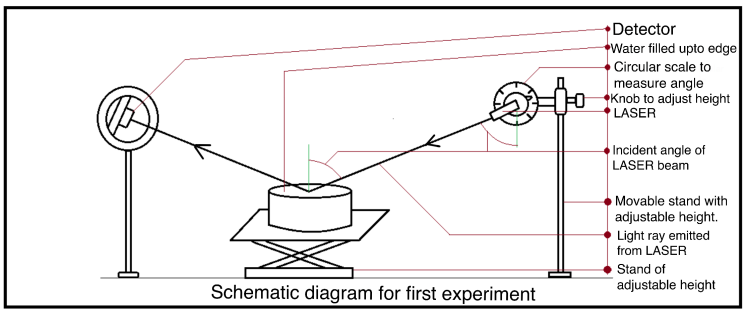

Figure 4. Apparatus for measuring reflectivity at different angles of incidence

We first give detailed measurements for the air-acrylic interface. Table 1 gives the data where

reflected intensity is measured in terms of the current in the CCD detector with proper calibration. Dark current was properly accounted for. Refracted intensity was inferred by subtracting the reflected intensity. Direct measurement of refracted intensity could not be done due to various difficulties (such as strong scattering of light in the medium, we will discuss these issues in the last section). Figure 5 gives the data for reflected intensity as a function of incident angle. Our experiment was carried out without controlling the polarization of light, hence we give for comparison theoretical values (from Eq.(1)) for the two different polarizations. As we see, our results lie in between the two curves for the two polarizations. In Figure 6 we re-plot reflected intensity along with the refracted intensity (obtained by just subtracting the reflected intensity form the incident value). Though there is no new information in the figure, it is instructive to see that the intensity of refracted light drops to zero as the incident angle approaches 90^o, and the entire intensity is reflected back. This confirms that between two horizontal layers of different refractive indices, if a light ray is travelling nearly horizontal, i.e. tangential to layers then most of the light continues in the same medium and negligible proportion of intensity (approaching zero as incident angle approaches 90^o) is transmitted in the other medium. Figure 7 and Figure 8 show the observations for air-water interface. We do not give the corresponding table in this case as the required information is contained in these plots.

It is evident that, for 90^o incidence, the refracted light ray at angle θ_c predicted by Fermat's principle will carry zero intensity. As we discussed above, since time reversal symmetry of Fermat's principle does not take intensity into consideration, arguments based on Fermat's principle cannot explain bending of light after it becomes horizontal in a mirage.

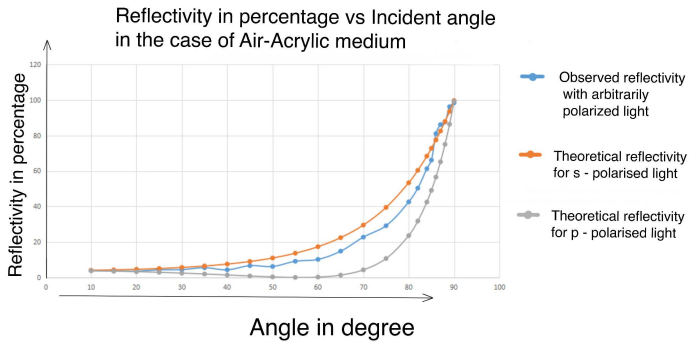

Figure 5. % Reflectance vs. incident angle for air-acrylic interface

4. THE ISSUE OF BENDING OF HORIZONTAL RAY IN GEOMETRICAL OPTICS

The crucial issue of the bending of the horizontal light in mirage was discussed by Raman and Pancharatnam [2, 3]. Here it was argued that the phenomenon of mirage cannot be described using geometrical optics. We reproduce here a summary of their arguments for this conclusion. They

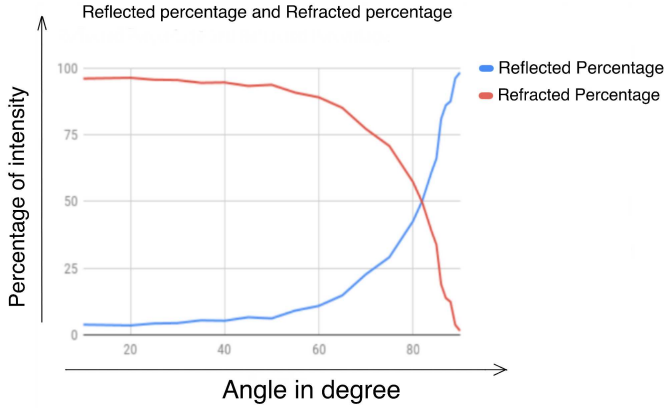

Figure 6. % Reflectance and % transmittance vs. incident angle for air-acrylic interface

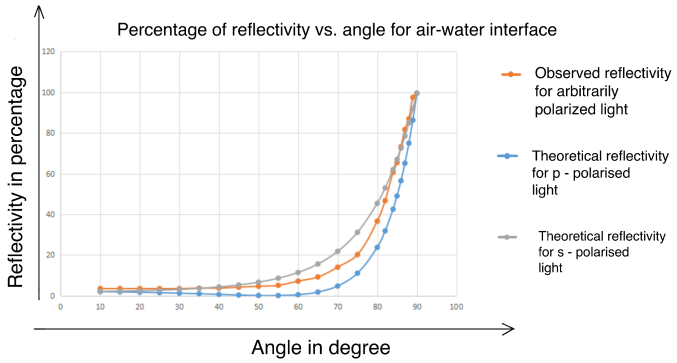

Figure 7. % Reflectance vs. incident angle for air-water interface

consider the medium as composed of several discrete thin layers, each of constant refractive index, which varies in the vertical direction. It is argued in [2, 3] that if an incident ray is making an angle (ϕ_1) with the plane of stratification then as the ray will continue through different mediums the angle (ϕ) will keep changing and after some time it will hit a limiting layer where μ_l=$\mu_1(\cos(\phi_1))$ (where μ_l is the refractive index of limiting layer and μ_1 is the refractive index of the first layer), according to Fermat's principle thence the ray should continue in a straight path. In other words, the total energy of the light will be confined in that infinitesimally thin layer and the intensity of the beam will be zero just below and above of that layer. It is shown in [2, 3] that proper explanation of the bending of horizontal ray (hence the phenomenon of mirage) can be obtained using wave optics.

We have argued above that application of Fermat's principle to determine the bending of transmitted light fails at critical angle. From the proper treatment of Maxwell's equations we saw that at critical angle the intensity of transmitted ray is zero and the total energy will be carried by the

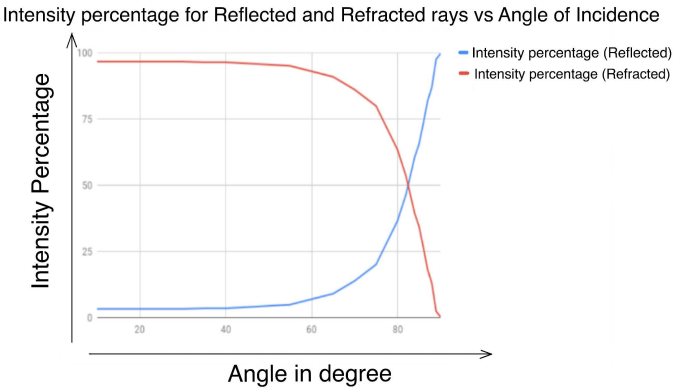

Figure 8. % Reflectance and % transmittance vs. incident angle for air-water interface

reflected ray. In other words there will be no horizontal ray for critical angle of incidence. In this context we note that the main source of the confusion about the role of horizontal ray originates from the conventional definition of the critical angle of incidence which is defined as *An angle of incidence for which the the angle of refraction is* 90°. In view of our discussion above pointing out that the transmitted ray in this case has zero intensity (actually existing only as an evanescent wave), this definition does not look very appropriate. A more appropriate (equivalent) definition for the critical angle would be *The minimum angle of incidence for which the intensity of the reflected ray is* 100% *of the incident ray* or in other words *The minimum angle for which light undergoes total internal reflection*.

Geometrical optics analysis of [2, 3] was questioned by Berry [1], basically arguing that in the case of mirage the ray actually never becomes horizontal, it just has a horizontal tangent at one point which is a very different situation than the ray being absolutely horizontal. Starting with the standard argument that a continuous refractive-index gradient curves a ray in a way that is analogous to the way the gravity bends the trajectory of a massive particle, the analysis in [1] considers the curved rays in a smoothly varying medium by caricaturing the refractive index profile as a stack of horizontal layers of thickness Δ. The refractive index μ is taken to be constant in each layer and limiting process $\Delta \to 0$ is examined using one of several possible discretizations. Here $\mu_{disc}(z) = \mu(z_n) = \mu(n\Delta) = \mu_n$ where n is an integer and $z_{n-1} < z \leq z_n$. So here the ray has also been divided into segments wth the horizontal location at the end of *m*th segment (Figure 9, see ref.[1] for details).

$$x_{N+m} = x_c + \sum_{l=1}^{m} X_l, \quad where\ X_l = \frac{K}{\sqrt{l-\gamma}} \quad and \quad K = \sqrt{\frac{\mu_c \Delta}{2\mu_c'}} \tag{4}$$

It is assumed that the limiting layer lies between the layers N and N+1, so the the critical layer is denoted as N+γ where $0 < \gamma \leq 1$. Now, one replaces the summation by integration and shows that

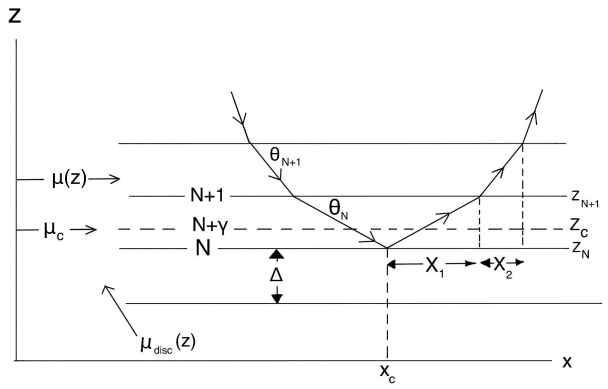

Figure 9. Trajectory of ray in discrete layered picture of mirage

the equation of the path of the ray will be

$$x(z) \approx x_c + 2k\sqrt{m} = x_c + 2k\sqrt{\frac{z - z_c}{\Delta}} = x_c + \sqrt{\frac{2\mu_c(z - z_c)}{\mu_c^{'}}} \tag{5}$$

Subsequent discussion in [1] discusses the limiting case for which $\Delta \to 0$ and $\gamma \to 1$ which is actually the situation envisaged by Raman. In that case in order to calculate the summation in Eq.(4), the l=1 term is separated due to problem when $\gamma \to 1$, and the summation is replaced by integration for other values of l. It is then argued that *For any fixed γ, however small, the term l=1 in the above summation vanishes as $\Delta \to 0$.* With that it is then shown that the ray will follow parabolic path.

It is certainly of crucial importance to understand the behavior of the $l = 1$ term for understanding the fate of the *horizontal* ray. It appears to us that the argument used in [1] for deciding the fate of horizontal ray using the limit $\Delta \to 0$ is not conclusive. We discuss this issue in the next section where we present our overall understanding about the issue of the horizontal ray.

5. THE HORIZONTAL INCIDENT RAY

As mentioned above, ref.[1] points out the issue of an important singular term in the bending equation of light. This issue remains unclear to us for the most general case of continuous bending of light. To have a well defined discussion, we consider a special situation, that of a light ray which is initially completely horizontal, propagating through a medium in which refractive index has only vertical gradient (say, increasing in downward direction for concreteness). For the ray optics approach of this problem we will consider Berry's argument and also the approach in [5].

First, we consider the equation of the location of *m*th segment in [1].

$$x_{N+m} = x_c + K \sum_{l=1}^{l=m} \frac{1}{\sqrt{l-\gamma}} \qquad where\ K = \sqrt{\frac{\mu_c \Delta}{2\mu_c'}} \tag{6}$$

It is also mentioned in [1] that the lowest ray for which l=1, can be arbitrarily long, we see that it tends to infinity as γ approaches 1 for the case of layered medium. This means that in the limit considered in [1], the horizontal location of the end of the *m*th segment which is given by

$$X_l = K \frac{1}{\sqrt{l-\gamma}} \tag{7}$$

should be tending to infinity for l=1 and γ tending to 1 for layered medium. For continuous medium however as Δ also tends to zero the limit becomes a $\frac{0}{0}$ condition and hence undefined. This suggests that although the ray will become horizontal and should not bend in this limiting condition for layered medium, this conclusion cannot be drawn for a continuous medium (with limit $\Delta \to 0$). However, for an initially horizontal ray, in layered picture $\gamma = 1$, exactly implying that the horizontal ray will not bend for any non-zero value of Δ.

We now consider the equation of bending of light as discussed in [5] where one starts with the differential equation for light ray given by $n\frac{d\vec{r}}{ds} = \vec{\nabla} S$. (We refer to [5] for details, here we only present explanation of terms relevant for our discussion.) The differentiation with respect to arc length s is taken on both of the sides leading to the equation

$$\frac{d}{ds}\left(n\frac{d\vec{r}}{ds}\right) = \vec{\nabla} n \tag{8}$$

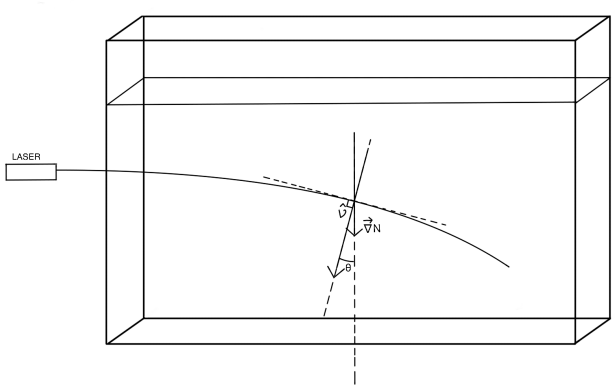

Figure 10. Light entering horizontal to the surface of layers

The curvature vector is defined to be $\vec{K} = \frac{1}{\rho}\vec{\nu}$ (see Figure 10) . Here $\vec{\nu}$ is the unit principle normal at that particular point. Then using Eqn.(8) and this definition of curvature, the general formula for the ray traveling in a medium with refractive index function n was derived. The differential equation of light rays after the inclusion of the curvature and taking the modulus value becomes

$$|K| = \frac{1}{\rho} = \vec{\nu}.\vec{\nabla}(ln\, n) \tag{9}$$

This equation shows that the refractive index increases as we move towards the principle normal which implies the bending of light ray towards the denser medium. The interesting thing here happens when we try to see this bending for a horizontal incident ray. For that case the direction of principle normal of a straight line is not defined. So we cannot use Eq.(9) to show the bending as the scalar product on the right side isn't defined. We can anyway use Eq.(8) for ray approximation. For that case $\vec{\nabla}n$ is zero. As the ray moves through just one medium in a plane of constant refractive index and is unable to *feel* the change of refractive index along the vertical direction. So using this we get

$$\frac{d}{ds}\left(n\frac{d\vec{r}}{ds}\right) = 0 \tag{10}$$

This equation gives a straight line solution which implies that the ray will not bend for this case. So we can see that the bending of a horizontal ray in a layered medium cannot be explained by these arguments. Here Raman's argument of wave optics is useful and can successfully show the bending of light. The symmetry in the case of ray approach for horizontal light in layered medium results in the straight line solution of those equations. Raman's wave argument has been discussed later. There are also conditions for the validity of geometric ray approach to this problem. As mentioned in [1–3] and also discussed in [5], the validity of ray optics requires that $\frac{\Delta n}{n} << 1$ for the length scale of wavelength of light in the medium. This brings us to the consideration of the gradient of the refractive index, which we address in the next section.

6. EXPERIMENTAL STUDY OF GRADIENT OF REFRACTIVE INDEX

It is standard to use a sugar solution with vertically varying concentration to realize the mirage situation in laboratory conditions. We used such a set up for investigating bending of light ray, especially focusing on the ray which is initially horizontal. A transparent cuboidal container is taken and saturated sugar solution is poured in its bottom. Now a layer of water is poured on top of this sugar solution and the interface of the two layers is stirred gently. A medium with gradient refractive index is obtained on letting this solution settle for some time. The method mentioned in [6] is adopted to determine the refractive index profile of the sugar solution prepared as we describe below.

A laser beam is passed through a glass rod (diameter around 1mm). The emerging fan of rays is then passed through the sugar solution and its image is obtained on a screen. The experimental arrangement is as shown in Figure 11.

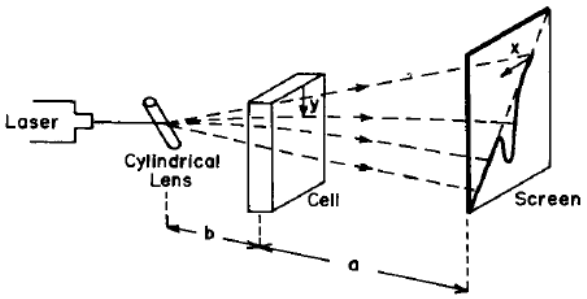

Figure 11. Schematic of the experimental arrangement

If the refractive index of the sugar solution was constant throughout its height, the image on the screen would have been a straight line. But the solution had gradient of refractive index which causes bending of light, and therefore the obtained image deviates from straight line. By measuring this deviation (Figure 12), rate of change of refractive index with height, dn/dy, can be calculated using the following formula.

$$\frac{dn}{dy} = \frac{z}{at} \tag{11}$$

where n is the refractive index, y is the height, z is the deflection on the screen with respect to straight line, t is the thickness of the cell or container in which the sample solution is kept, and a is the distance of the screen from the cell. Approximation involved in the derivation of equation 11 is that the thickness t is small [6] (so that relative deflections remain small). We have used thickness t $\simeq$ 18 mm for the experiment. Fig.13 shows the image obtained on the screen (for the blue laser) for the sugar solution used in our set up. Analyzing Figure 13 with equation 11, we obtain the profile of the refractive index gradient dn/dy as shown in Figure 14 for the solution used for the study.

As we discussed in the previous section, the crucial issue is to understand the bending of a ray which is initially horizontal. As expected, we observe that when a horizontal beam of light enters the sugar solution, it bends towards the direction of increasing refractive index (Figure 15). Trajectory of the light beam was also studied for the case when light enters the sugar solution at an angle (Figure 16). In all these cases, bending of light is more where dn/dy is large.

We also see that the sugar solution introduces magnification of the light beam as light passes through it due to the gradient of refractive index. Different dn/dy gave different magnification of the beam. Figure 17 is the image obtained on the screen after light passes through the maximum dn/dy region. The main purpose for measuring dn/dy was to probe the condition for the validity

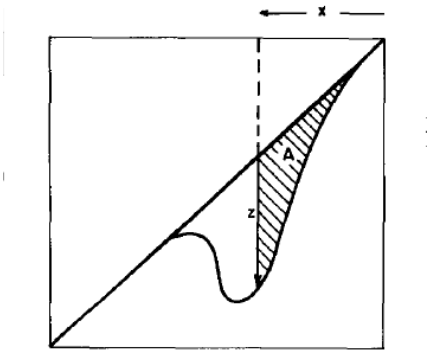

Figure 12. The initial and deflected beam trace on the screen

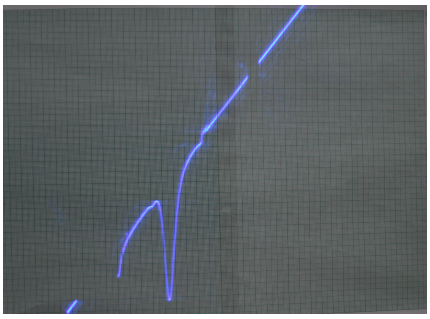

Figure 13. Image obtained on the screen which is then used for determining refractive index gradient throughout the height of solution

of geometrical optics which, as we mentioned above, requires that $\frac{\Delta n}{n} << 1$ for the length scale of wavelength of light in the medium. We expect that the intensity of the transmitted light (the ray which is bending, starting with horizontal direction) should show qualitative changes as one crosses this condition. For this purpose we measured dn/dy for different wavelengths. Unfortunately, it was not possible to measure the intensity of the transmitted light due to strong scattering of light from the medium as well as a very significant spread of intensity in the vertical direction. This is seen in the left two pictures in Figure 17 where one can see the spread of the beam profile in vertical direction. Because of this we were unable to complete the investigation of the intensity of transmitted light depending on dn/dy and the wavelength of light. We still provide the results of our investigations to make the reader familiar with the very useful technique of [6] for measuring refractive index gradients. Also, hopefully our study provides a platform for conducting further experimental investigation of the bending of horizontal light in the regime of refractive index gradient which crosses the limit for the validity of geometrical optics.

As we mentioned, the relevant quantities for our investigations are dn/dy and the wavelength

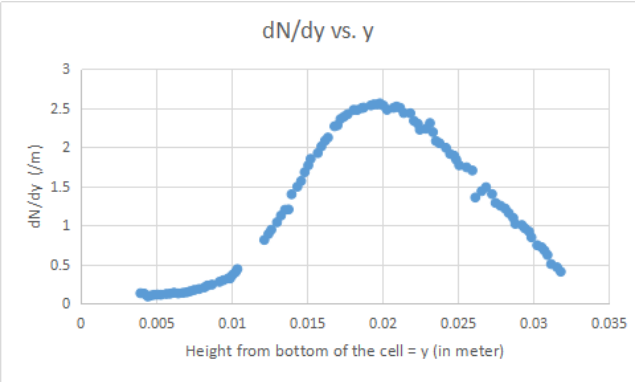

Figure 14. Refractive index gradient vs. height of liquid from bottom of container

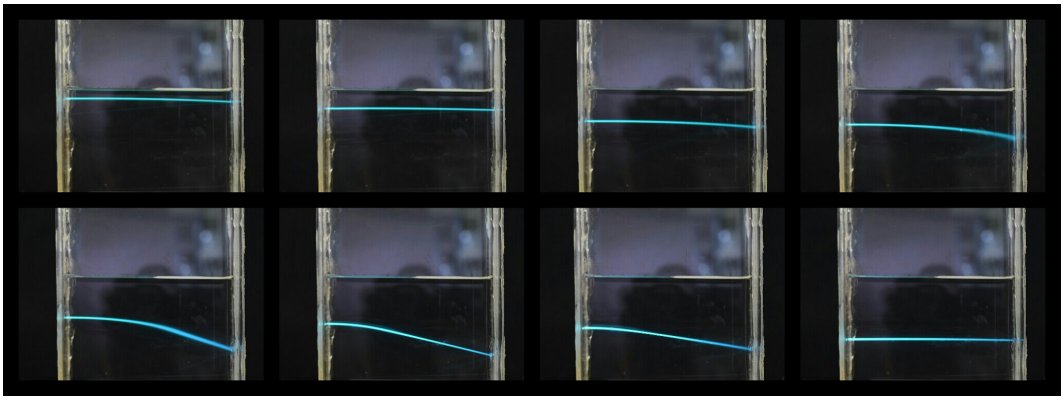

Figure 15. Trajectory of light entering horizontally in sugar solution (light beam is entering from left)

of light. To that purpose, we have repeated the experiment for measurement of dn/dy with different color lasers. Two laser beams of different colors were overlapped using a beam-splitter which was then passed through a glass rod to generate a fan of rays. We observed that the smaller wavelength light bent more. And this was observed only around the region where dn/dy was maximum. Third picture from left in Figure 17 shows that bending of blue light is more than that of red light when passing through the layer of maximum dn/dy, while the right most picture in Figure 17 shows the separation of constituent colors of white light when it is passed through the layer of maximum dn/dy. Here also blue light bends more. Since bending (i.e. deflection) is directly proportional to dn/dy, the observation implies that dn/dy for blue is more than that for red in the layer of maximum dn/dy as one will expect.

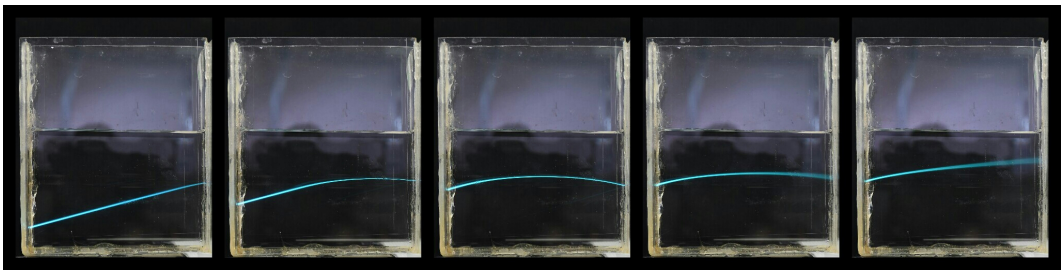

Figure 16. Trajectory of a light beam entering obliquely in sugar solution (light beam is entering from left)

7. SUMMARY AND CONCLUSIONS

We have argued above that for the case of horizontal incident ray the ray optics approach fails to show the bending of light. A satisfactory explanation of this bending was discussed by Raman and Pancharatnam [2, 3]. They considered the light to be a wave which propagates in the x direction and whose amplitude changes along z direction. The grading of refractive index is in the z direction. So the wave was described by the function $\psi = e^{ikpx}u(z)$. Here u(z) is the z dependent amplitude. Then by using general wave equation solution the intensity distribution of light as a function of distance from the limiting layer was derived. Using wave optics Raman and Pancharatnam explained all the phenomena observed experimentally. We refer to ref.[2, 3] for details of this approach.

For the conventional explanation of mirage within geometrical optics approach we have argued that the treatment of the horizontal section of the light ray requires crucial inputs from wave optics. We have argued that the standard approach of focusing on refracted ray cannot lead to correct understanding of mirage in the geometrical optics framework. What one needs is that at certain point during the bending trajectory of light, one needs to switch attention to the reflected light (which carries the entire intensity of incident light in that part of the medium, while any refracted light continues with zero intensity). This reflected light then propagates upwards undergoing refraction through successive layers. This refracted component continues bending upward, finally leading the the standard mirage. The standard derivations uses the bending of only transmitted light obtained from Eq.(3) with the application of Fermat's principle. Hence, one will expect that there must be some difference in the light trajectory if we require that one switches attention to the reflected ray instead of continuing to follow up of the transmitted ray via Fermat's principle, especially near the horizontal segment. It will be an interesting problem to find any such differences and try to carry out experimental observation of that. We hope to carry out such an investigation in future.

To have well defined discussion, especially in view of the singularity in the equation for bending of light as pointed out in [1], we have focused on a light ray which is initially horizontal. We have analyzed this situation within the geometrical optics framework as discussed in [1, 5] and have discussed the difficulties in understanding the bending of such a ray. Both the cases of mirage and horizontal incident beam can be well explained by wave theory of light. If the refractive index varies

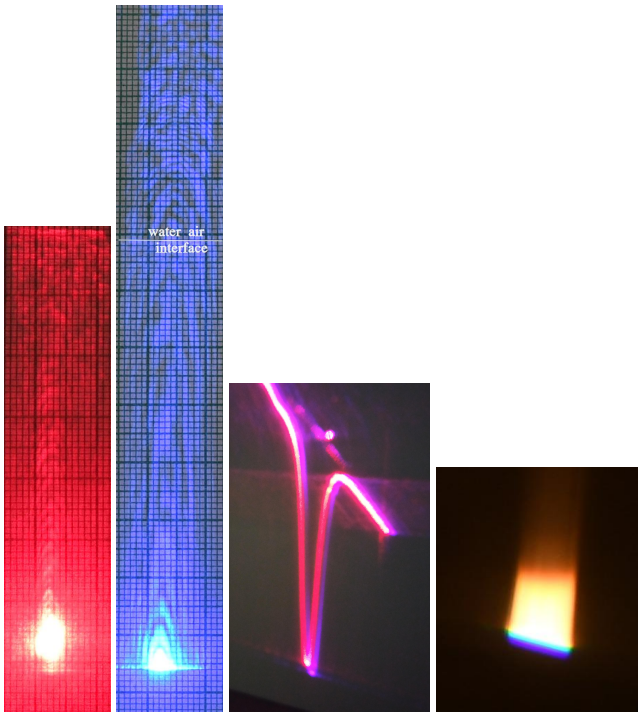

Figure 17. Left two pictures show the vertical spread of intensity after light beam passes through the sugar solution around the region of maximum dn/dy (with red and blue LASER respectively). Third picture from left shows that bending of blue light is more than that of red light when passing through the layer of maximum dn/dy, while the right most picture shows the separation of constituent colors of white light when it is passed through the layer of maximum dn/dy. Here also blue light bends more.

significantly in the range of the wavelength of light then ray treatment will be strictly invalid. Several factors may be important for this discussion, for example the behavior of intensity of the horizontal ray resulting from a ray incident at critical angle from denser to rarer medium (with sharp interface) needs to be studied in the presence of several layers, within the range of the wavelength of light. This will more closely represent the situation of a continuously varying refractive index medium. The evanescent wave nature of this horizontal transmitted ray may be important in such a situation. One needs to carry out controlled experimental study of the changes in the intensity of transmitted light along the bending curve when dn/dy is increased crossing the validity of geometrical optics regime.

ACKNOWLEDGEMENT

We are very grateful to Rajaram Nityananda for very insightful discussions on this topic and for making us aware of refs.[1–3]. We are also grateful to the National Initiative on Undergraduate Science (NIUS) at the Homi Bhabha Centre for Science Education, TIFR, Mumbai, India, for providing the required facilities, staff and funding for the study. The authors are thankful to the NIUS (Physics) laboratory staff for all their help. We are also thankful to IOP, Bhubaneswar for providing facilities during a visit of some of the authors for this project.

References

[1] M. V. Berry, "Raman and the mirage revisited: confusions and a rediscovery", Eur. J. Phys. 34, 1423 (2013)

[2] C.V. Raman and S. Pancharatnam, "The optics of mirages" Proc. Ind. Acad. Sci. A49, 251 (1959)

[3] C.V. Raman, "The optics of mirages", Curr. Sci. 29, 309 (1959)

[4] John David Jackson, "Classical Electrodynamics", 3rd edition, Page 305-306

[5] Max Born and Emil Wolf, "Principles of optics", Cambridge University Press, 7th edition

[6] A. J. Barnard, and B. Ahlborn, "Measurement of refractive index gradients by deflection of a laser beam", American Journal of Physics 43, 573 (1975)

Data of reflected and refracted light intensity by air-acrylic surface						Theoretical % reflectivity for	
Angle	Dark current (A)	Current (A) (Reflected)	Net current(A)	Percentage of reflected current	Percentage of refracted current	s- polarised	p- polarised
10	0.07	2.7	2.63	3.845	96.155	4.051	3.729
15	0.07	2.6	2.53	3.698	96.302	4.263	3.530
20	0.07	2.5	2.43	3.552	96.448	4.581	3.249
25	0.07	3	2.93	4.283	95.717	5.025	2.887
30	0.07	3.1	3.03	4.429	95.571	5.629	2.448
35	0.07	3.8	3.73	5.453	94.547	6.441	1.939
40	0.07	3.7	3.63	4.307	95.693	7.528	1.380
45	0.07	4.6	4.53	6.622	93.378	8.987	0.812
50	0.07	4.3	4.23	6.184	93.816	10.958	0.309
55	0.07	6.3	6.23	9.108	90.892	13.642	0.014
60	0.07	7.5	7.43	10.162	89.838	17.327	0.189
65	0.07	10.2	10.13	14.809	85.191	22.427	1.312
70	0.07	15.6	15.53	22.704	77.296	29.530	4.259
75	0.07	20	19.93	29.137	70.863	39.465	10.657
80	0.07	29.2	29.13	42.587	57.413	53.376	23.587
82	0.07	34.5	34.43	50.336	49.664	60.382	31.780
84	0.07	42	41.93	61.301	38.699	68.383	42.510
85	0.07	45.3	45.23	66.125	33.875	72.796	49.064
86	0.07	55.5	55.43	81.038	18.962	77.508	56.571
87	0.07	59	58.93	86.154	13.846	82.536	65.172
88	0.07	60	59.93	87.616	12.384	87.899	75.035
89	0.07	65.9	65.83	96.242	3.758	93.618	86.355
90	0.07	67.4	67.33	98.435	1.565	99.712	99.362
					Max. current = 0.0684 mA		

Table 1. Observations of Exp. 1 for air-acrylic surface

STUDENT JOURNAL OF PHYSICS

Volume 7 **Number 4** **Oct - Dec 2018**

CONTENTS

ARTICLES